Spatial evidence of cryptic methane cycling and methylotrophic metabolisms along a land-ocean transect in a California coastal wetland

Sebastian J.E. Krause[1a], Rebecca Wipfler[3], Jiarui Liu[1], David J. Yousavich[1], De'Marcus Robinson[2], David W. Hoyt[4], Victoria J. Orphan[3], and Tina Treude[1,2]

[1]Department of Earth Planetary and Space Sciences, University of California, Los Angeles, CA 90095, USA

[2]Department of Atmospheric and Ocean Sciences, University of California, Los Angeles, CA 90095, USA

[3]Division of Geological and Planetary Sciences, California Institute of Technology, Pasadena, CA 91125, USA

[4]Pacific Northwest National Laboratory Environmental and Molecular Sciences Division, Richland, WA 99352, USA

Corresponding author: Sebastian J. E. Krause; sjkrause@ucsb.edu

[a]Present address: Earth Research Institute, 6832 Ellison Hall, University of California Santa Barbara, Santa Barbara, CA 93106-3060, USA

Keywords: Sulfate reduction; Iron reduction; Mono-Methylamine; Methanol; Acetate; Salt Marsh; Metabolic activity; Radiotracer; Methanogenesis; Anaerobic Oxidation of Methane

Abstract

Methylotrophic methanogenesis in the sulfate reduction zone of wetland and marine sediment has recently been coupled to anaerobic oxidation of methane (AOM), now referred to as the cryptic methane cycle. In this study we present evidence of cryptic methane cycling activity within the sulfate-reducing zone, along a land-ocean transect within the Carpinteria Salt Marsh Reserve (CSMR), Carpinteria, CA, USA consisting of four stations; two brackish, one marine, and one hypersaline. The top 20 cm of sediment collected along the transect was subjected to geochemical and molecular analysis, in vitro methanogenesis batch incubations, and radiotracer incubations using $^{35}S\text{-}SO^{2-}_4$, ^{14}C-mono-methylamine, and $^{14}C\text{-}CH_4$ to find evidence of cryptic methane cycling activity. Results showed that subsurface porewater salinity increased with increasing sediment depth in the two brackish stations while remaining close to saline or hypersaline in the other stations, suggesting complex subsurface hydrology across the CSMR. Methane concentrations were consistently low (3 to 28 µM) except at the marine station, which showed increasing methane with increasing sediment depth (max 665 µM). In vitro methanogenesis batch incubations showed no linear build-up of methane over time, except with sediment from deeper intervals at the marine station, suggesting a process that is limiting methane production in the sediment. AOM rates from direct measurements with $^{14}C\text{-}CH_4$ were low in the two brackish and hypersaline stations (0.03 to 0.66 nmol cm^{-3} d^{-1}) while at the marine station AOM rates increased with increasing sediment depth (Max 19.4 nmol cm^{-3} d^{-1}). Total organic carbon (TOC) and total organic nitrogen (TON) were highest in the sediment intervals near the surface at the two brackish stations and hypersaline station, while at the marine station TOC and TON were higher towards the bottom of the core (<0.5% to 5.4% for TOC and 0.02% to 0.38% for TON). Porewater sulfate concentrations were never limiting (9 to 91 mM) across

the transect despite sulfate reduction actvity (1.5 to 2506 nmol cm^{-3} d^{-1}) in sediment intervals near the surface. Porewater sulfide and iron (II) profiles revealed that the sediment transitioned from predominantly iron-reducing to a predominantly sulfate-reducing between the two brackish stations and the marine and hypersaline stations. Metabolomic analysis of porewater revealed that substrates for methanogenesis (i.e., acetate, methanol, and mono-methylamine) were mostly below detection, but some samples from the 0-1.5 cm, 9.5-10.5 cm, and 14.5-15.5 cm depths showed non-quantifiable amounts of mono-methylamine and methanol, indicating rapid turnover of these substrates. Acetate had quantifiable amounts in some depth intervals at most stations ranging between 45 and 72 µM. Estimated methanogenesis from mono-methylamine was detected throughout the sediment at all stations, with the highest rates found in intervals close to the surface, ranging between 0.14 and 3.8 nmol cm^{-3} d^{-1}. Differences between the rate constants (k) of methanogenesis from ^{14}C-mono-methylamine and AOM from either direct injection of ^{14}C-CH_4 or ^{14}C-mono-methylamine derived ^{14}C-CH_4, point towards a separate metabolic process activity metabolizing mono-methylamine to inorganic carbon. Molecular analysis revealed that microbial communities at the two brackish stations are closer related to each other than the communities at the marine and hypersaline stations. Molecular analysis also revealed the presence and overlap of methanogenic and anaerobic methanotrophic archaea but only in the marine and hypersaline stations, suggesting that the two organisms are involved with cryptic methane cycling either as a couple or by methanogenic archaea capable of both methanogenesis and AOM. Orders within the Desulfobacterota phylum capable of sulfate and iron reduction were detected throughout the sediment and are potentially responsible for sulfate reduction rates and buildup of reduced iron across the transect. We conclude that the results in this work show strong evidence of cryptic methane cycling activity in the top 20 cm of sediment in the CSMR. Based

off the evidence the cryptic methane cycle is likely preventing major buildup of methane in the sulfate-reducing zone due to rapid cycling of carbon between methanogenesis and AOM. Our data revealed methanogenic and anaerobic methanotrophs are present in the CSMR which are likely responsible for cryptic methane cycling. Furthermore, our data point towards methylamine utilization by both methanogenic archaea and non-methanogenic microorganisms in the CSMR. We hypothesize that sulfate reduction, by groups of sulfate-reducing bacteria, is actively consuming methylamine alongside methanogenic archaea, but additional work is needed to confirm this metabolic activity and identify who is responsible.

1. Introduction

Methane is the simplest and most abundant organic molecule in the atmosphere and is 25 times more potent than carbon dioxide as a greenhouse gas (Ipcc, 2014). Since pre-industrial technological advancement, methane concentrations in the atmosphere have doubled from 722 ppb to approx. 1850 ppb in 2017. Saunois et al. (2020) reported that natural wetlands between the years 2008-2017 contributed on average 142 Tg CH_4 yr^{-1} (range between 102-182 Tg CH_4 yr^{-1}) which makes natural wetlands the largest contributor of methane into the atmosphere. Natural wetlands are broadly characterized into freshwater and coastal wetlands. Both ecosystems contain organic-rich sediment that could sustain microbial methanogenesis. However, coastal wetlands, such as estuaries, tidal pans and salt marshes, emit far less methane into the atmosphere (1.3 g CH_4 m^{-2} yr^{-1}) than freshwater wetlands (7.1 g CH_4 m^{-2} yr^{-1}) (Bridgham et al., 2006; Bridgham et al., 2013). The lower methane emission is due to the presence of sulfate which enters coastal wetlands via marine seawater inflow and mixes with freshwater inflows creating distinct salinity gradients in the overlying water (Reddy et al., 2022). Salinity in the sediment of coastal wetlands is mostly driven by daily tidal influence (Del Pilar Alvarez et al., 2015; Reddy et al., 2022; Gardner, 2007; Li et al., 2023; Moffett et al., 2010) but also wetland geomorphology, sediment characteristics, climate conditions (Montalto et al., 2006), evapotranspiration, bioturbation (Carol et al., 2011; Cao et al., 2012; Li et al., 2023), and anthropogenic alterations (Carol et al., 2012). The sulfate that enters wetlands' sediment porewater, supports microbial sulfate reduction and thereby suppresses competitive methanogenesis pathways (hydrogenotrophic and acetoclastic) (Kristjansson et al., 1982; Winfrey and Ward, 1983; Lovley and Klug, 1986; Jørgensen, 2000). As a result, methane tends to buildup in deeper anoxic sediment below the sulfate penetration depth, and thus no sulfate

reduction activity. In the lower portion of the sulfate reduction zone, where the concentration of sulfate is decreasing and overlaps with increasing methane concentration is a sediment zone known as the sulfate methane transition zone (SMTZ), where anaerobic oxidation of methane (AOM) occurs (Hinrichs and Boetius, 2002; Reeburgh, 2007; Knittel and Boetius, 2009). In the SMTZ, AOM oxidizes methane with sulfate as the electron acceptor and has been shown to consume up to 96% of methane before reaching the water column within anoxic coastal wetland sediment (La et al., 2022). The process is typically mediated by a consortium of anaerobic methane-oxidizing archaea (ANME) and sulfate-reducing bacteria (Knittel and Boetius, 2009; Orphan et al., 2001; Michaelis et al., 2002; Boetius et al., 2000; Hinrichs and Boetius, 2002; Reeburgh, 2007).

Although sulfate reduction outcompetes methanogenesis for hydrogen and acetate in the sulfate reduction zone above the SMTZ, methylated substrates such as methylsulfides, methanol and methylamines, are known to be non-competitive for methanogenesis of the methylotrophic pathways (Oremland and Taylor, 1978; Lovley and Klug, 1986; Maltby et al., 2016; Zhuang et al., 2016; Zhuang et al., 2018; Krause and Treude, 2021; Krause et al., 2023). Thus, methylotrophic methanogenesis activity has been shown to occur within the sulfate-reducing zone in various aquatic environments, including coastal wetlands (Oremland et al., 1982; Oremland and Polcin, 1982; Krause and Treude, 2021). However, despite the methylotrophic methanogenesis activity, methane concentrations are by several orders of magnitude lower within the sulfate-reducing zone, above the SMTZ, compared to deeper sediments where sulfate is depleted (Barnes and Goldberg, 1976; Wehrmann et al., 2011; Beulig et al., 2018; Krause et al., 2023; Krause and Treude, 2021). This low level of methane is controlled by concurrent methylotrophic methanogenesis and AOM activity which is now referred as the cryptic methane

cycle, and has been detected in the marine and coastal wetland sediment (Krause and Treude, 2021; Xiao et al., 2017; Xiao et al., 2018; Krause et al., 2023).

Important questions remain about how methane is cycled in coastal wetlands across salinity gradients and electron acceptor availability. Moreover, the microbial communities, that may be involved directly or indirectly with the cryptic methane cycle have not been identified. Coastal wetlands are ideal geographical features to study these questions because of their unique hydrology where freshwater and marine sources interact creating natural gradients between salinity and terrestrial input, which potentially affects the availability of important electron acceptors (e.g., sulfate, iron (III), nitrate) and the related microbial communities that drive cryptic methane cycling. Therefore, it is crucial to investigate the biogeochemical trends, the metabolic activity of methanogenesis, AOM and sulfate reduction, as well as the shift in microbial communities along a natural salinity gradient of coastal wetlands.

The primary objective of the present study is to provide new evidence of cryptic methane cycling along a spatial transect following a natural salinity gradient in a California coastal wetland, the Carpinteria Salt Marsh Reserve (CSMR). Thereby, we aim to elucidate the availability of electron acceptors that drive AOM, and to characterize the microbial communities that are responsible for cryptic methane cycling. In the following study we will show concurrent activities of methanogenesis and AOM, along with potential microbial communities involved, within sulfate-rich sediment across the CSMR land-ocean transect, which strongly suggest active cryptic methane cycling. In addition, our finds point to an active non-methanogenic anaerobic methylotrophic metabolism alongside the cryptic methane cycle.

2. Methods

2.1. Study area and field study

The field site focused on this study is the Carpinteria Salt Marsh Reserve (CSMR), which is located about 15 km east of Santa Barbara, California USA and is part of the University of California Natural Reserve system. Within the CSMR, three freshwater streams flow from the North to the South and open into the Pacific Ocean (Fig. 1). Seawater does infiltrate the CSMR through daily tidal fluxes and mixes with freshwater that enters the CSMR from the North. The mixing results in a natural salinity gradient in the surface waters during low tide. In summer of 2019, sediment samples for this study were collected from a total of four stations (three inside connected creeks and one inside an isolated pool) within the CSMR along a land-ocean, i.e., North-South, transect featuring differences in salinity in the supernatant water. Stations were picked based on accessibility and the salinity of the overlying water during low tide, measured in the field with a hand-held refractometer. The stations include brackish low (BL, 7 PSU), brackish high (BH, 15 PSU), marine (M, 35 PSU), and hypersaline (HP, 139 PSU) conditions. The hypersaline conditions are linked to an isolated, evaporative pool, which has been studied previously (Krause and Treude, 2021).

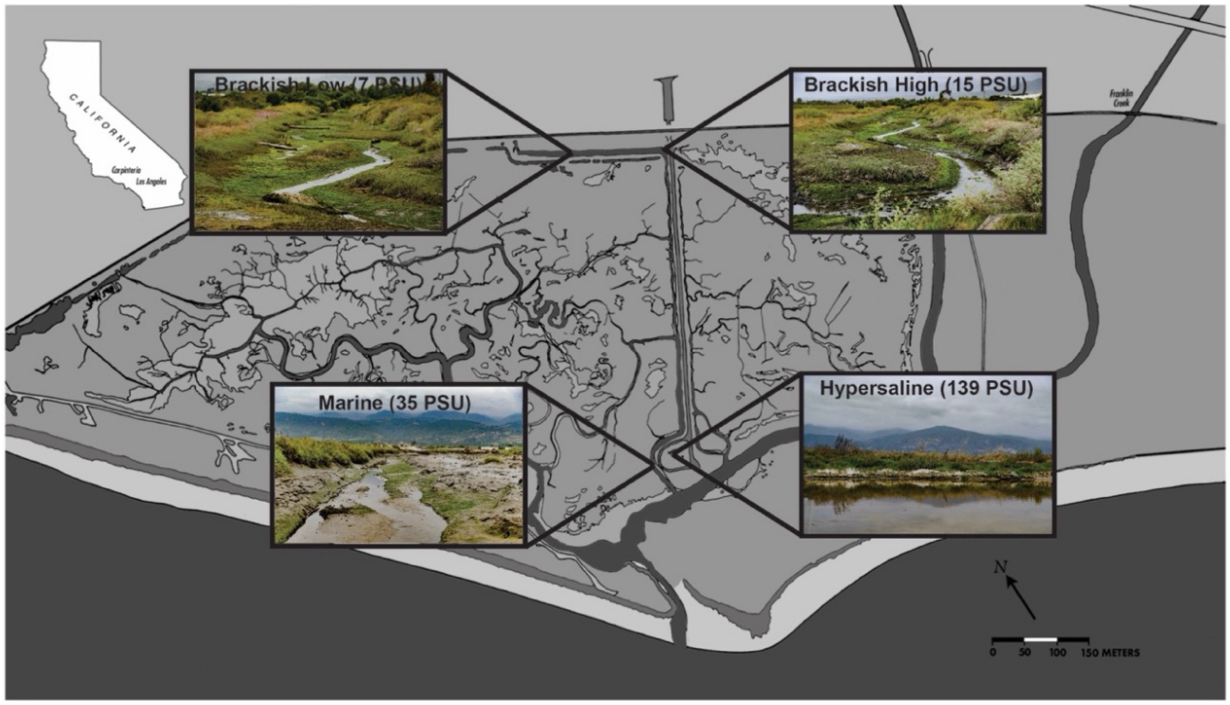

Figure 1. Map of the Carpinteria Salt Marsh Reserve and with sampling locations along the natural salinity gradient. The Brackish Low, Brackish High and Marine stations are connected via creeks; the Hypersaline station is an evaporative isolated pool. PSU = practical salinity units.

The top 15 to 20 cm of sediment at each station was collected in large (10 cm i.d.) and small (2.6 cm i.d.) polycarbonate push cores. Push cores were carefully inserted into sediment by hand including approximately 5 cm overlying water. Large push cores were inserted approximately 20 cm from each other, while small push cores were inserted approximately 15 cm from each other to provide sufficient space for push core excavation and extraction. Sediment surrounding the push cores was carefully removed to place a metal plate under the bottom to safely extract the push cores. Any air headspace within the push cores were filled bubble-free with overlying-water from the station location along the creek or hypersaline pool and sealed with rubber stoppers and electrical tape. Sediment push cores were transported to the home laboratory on the same day, stored in the dark at room temperature and processed within 1 d to 1 week of collection, depending on the analysis type (see 2.2 – 2.7).

2.2. Porewater geochemistry and solid phase analysis

One day after collection, one large push core from each station was selected for porewater geochemistry analysis. At stations BL, BH, and M the sediment was sliced in 1 cm increments, while the top layer of the HP station was sliced at 1.5 cm followed by 1 cm increments due to a natural slope found at the sediment surface during the time of sampling. All sediment was sliced under a constant flow of argon gas to minimize oxidation of oxygen-sensitive substrates. The sediment sections were transferred to pre-argon flushed 50 mL centrifuge vials and centrifuged at 4300 *g* for 20 mins. Immediately after centrifugation, the separated porewater was analyzed spectrographically for dissolved sulfide according to (Cline, 1969) and iron (II) according to (Grasshoff et al., 1999) using a Shimadzu UV-Spectrophotometer (UV-1800) equipped with a sipper unit. The remaining porewater was frozen (-30 °C) and later measured for dissolved porewater sulfate and chloride concentrations. Porewater sulfate and chloride was determined using an ion chromatograph (Metrohm 761) (Dale et al., 2015). Analytical precision of these measurements was <1% based on repeated analysis of IAPSO seawater standards. Absolute detection limit of sulfate was 1 μM, which corresponds to 30 μM in the undiluted sample. Porewater salinity at each station was calculated from chlorinity using Knudson's equation (Salinity = 1.805 * Chlorinity) assuming that the major ionic ratios in the porewater and in seawater are similar (Knudsen, 1901). One mL of porewater was subsampled for the determination of methylamine concentrations and other methanogenic substrates (see section 2.4).

For methane concentrations, porosity/density, solid-phase carbon/nitrogen analysis, and molecular analysis, a separate large push core from each station the top 1.5 cm was sliced followed by 1 cm increments because of natural slopes at the sediment surface found at the time of sampling. For methane concentrations, 2 mL of sediment at each 1 cm interval was

subsampled using a 3 mL cut-off plastic syringe and transferred to a 12 mL glass serum vial filled with 5 mL of 5% NaOH and sealed with grey butyl rubber stoppers. Headspace methane concentrations were later determined using a Shimadzu gas chromatography (GC-2014) equipped with a packed Haysep D and flame ionizer detector. The column was heated to 80 °C and ultra-high pure helium was used as the carrier gas, set to 12 mL per minute. A methane standard (Scotty Analyzed Gases) was used to calibrate for methane concentrations with a ± 5% precision.

For porosity and density, 8 mL of sediment was collected from each 1 cm layer using a 10 mL plastic cut off syringe, transferred to pre-weighed plastic 10 mL vials (Wheaton). The wet samples were then weighed and then stored at 4 °C. The samples were later dried at 75 °C for 72 hrs and then reweighed. Sediment porosity was determined by subtracting the dry sediment weight from the wet sediment weight and dividing by the total volume. Sediment density was determined by dividing the wet weight by the total volume of the sample.

Analyses for sediment total organic carbon (TOC) and total organic nitrogen (TON) were modified from (Harris et al., 2001). Briefly, samples were dried up to 48 hours at 50°C until the dry weight was stable and then treated with direct addition of 1 mL of 6N HCl to dissolve carbonate minerals. These samples were then washed in triplicate with 1-mL of ultrapure water or until a neutral pH was re-established. Samples were centrifuged at 4255 X *g* for 20 minutes, the supernatant was decanted, and vials were re-dried at 50°C. A subsample (approx. 10-15 mg) was then packed into individual 8x5 mm pressed tin capsules and sent to the University of California Davis Stable Isotope Facility for analysis using Elemental Analyzer – Isotope Ratio Mass Spectrometry. TOC and TON were calculated based on the sample peak area corrected against a reference material (alfalfa flour).

For molecular analysis, 2 sets of 3 mL of sediments were collected using a 3 mL plastic cut-off syringe into 3 mL plastic cryo vials and immediately stored at -80°C for further analysis (see section 2.9 for details).

2.3. In-vitro net methanogenesis

One week after sample collection, one large push core from each station was selected to study in-vitro methanogenesis in the natural sediments. Between 2 and 3 sediment intervals at each station were selected and subsampled for this analysis based on porewater geochemistry and solid-phase analysis (see details in Fig. 3).

Sediment subsampling was performed similarly to section 2.2. Each push core was sliced at the designated sediment layers under a constant flow of argon to minimize oxygen poisoning of anaerobic microbial communities within the sediment. Using a 3 mL plastic cut-off syringe, 10 mL sediment from each interval was transferred into triplicate sterilized, argon-flushed 60 mL glass serum vials. Vials were sealed with blue butyl rubber stoppers (Bellco Glass Inc, 20 mm diameter) and crimped with aluminum crimps. The headspace of each vial was flushed with argon for one minute to remove oxygen. The vials were then incubated in the dark, at room temperature and monitored for 22 days. Methane concentrations in the headspace were tracked using a gas chromatograph (see section 2.2).

2.4. Metabolomic analysis

Sediment porewater concentrations of methanogenic substrates (methylamine, methanol, and acetate), were obtained from a selection of depth intervals at each station (see specifics in section 3.1.4.) by syringe-filtering (0.2 µm) 1 mL porewater into pre-combusted (350 °C for 3 hrs) amber glass vials (1.8 mL). Samples were then closed with screw caps equipped with a PTFE septa and frozen at -80 °C until analyses. Samples were analyzed at the Pacific Northwest

National Laboratory, Environment and Molecular Sciences Division for metabolomic analysis using proton nuclear magnetic resonance (NMR). For details on sample preparation and analysis see section 2.4 in Krause et al. (2023).

2.5. Sulfate reduction (^{35}S-Sulfate)

Within one day of collection, one small sediment whole round push core from each station was used to determine sulfate-reduction rates (SRR) at the home laboratory. Radioactive, carrier-free ^{35}S-sulfate ($^{35}S\text{-}SO_4^{2-}$; dissolved in MilliQ water, injection volume 10 µL, activity 260 KBq, specific activity 1.59 TBq mg^{-1}) was injected into the whole-round cores at 1 cm intervals and incubated at room temperature and in the dark following (Jørgensen, 1978). The incubation was stopped after ~24 hours. Sediment samples (including controls) were transferred, preserved, and stored according to Krause and Treude (2021). Samples were analyzed using the cold-chromium distillation method and the results from the analysis were used to calculate the sulfate reduction rates according to (Kallmeyer et al., 2004).

2.6. Methanogenesis and AOM from mono-methylamine

The present study aimed to follow the methane production by methanogenesis from mono-methylamine (hereafter abbreviated MG-MMA) and the subsequent oxidation of the methane to dissolved inorganic carbon (DIC) by anaerobic oxidation of methane (hereafter abbreviated AOM-MMA) (i.e., cryptic methane cycling) in salt marsh sediments across a salinity gradient. To find evidence of concurrent MG-MMA and AOM-MMA, one small whole round core from each station was injected with radiolabeled ^{14}C-mono-methylamine (^{14}C-MMA) (^{14}C-mono-methylamine dissolved in 1 mL water, injection volume 10 µL, activity 220 KBq, specific activity 1.85-2.22 GBq mmol^{-1}) at 1-cm intervals according to (Krause and Treude, 2021) and stored at room temperature and in the dark for 24 h. Incubations were terminated by slicing the

sediment at 1-cm intervals into 50 mL wide-mouth glass crimp vials filled with 20 mL of 5% NaOH. After transfer of the sample, vials were immediately sealed with a red butyl stopper and crimped with an aluminum crimp. Control samples were prepared by sectioning the top 5 cm of a separate whole round core from each station in 1-cm intervals into 50 mL wide mouth vials filled with 20 mL of 5% NaOH prior to radiotracer addition. Vials were shaken thoroughly for 1 min to ensure complete biological inactivity and stored upside down at room temperature till further processing. The residual ^{14}C-MMA in the liquid, the ^{14}C-CH_4 in the headspace of the sample vials produced by MG-MMA, and the ^{14}C-TIC in the sediments as a result of AOM-MMA samples were determined by the analysis according to (Krause and Treude, 2021).

To account for the ^{14}C-MMA binding to mineral surfaces (Wang and Lee, 1993, 1994; Xiao et al., 2022), we determined the recovery factor (RF) for the sediment from stations BL, BH and M following the procedure of Krause and Treude (2021). For the HP station, the RF factor determined by Krause and Treude (2021) was applied.

Estimates of metabolic rates of MG-MMA and AOM-MMA were calculated from the results of the ^{14}C-MMA incubations. Natural concentrations of mono-methylamine in the sediment porewater were detectable (> 3 µM) but were below the quantification limit (10 µM) (See section 3.1.4). To enable rate calculations for MG-MMA (Eq. 1), we assumed an MMA concentration of 3 µM for all samples, i.e., the detection limits of the NMR analysis.

$$MG\text{-}MMA = \frac{a_{CH_4} + a_{TIC}}{a_{CH_4} + a_{TIC} + \left[\frac{a_{MMA}}{RF}\right]} * [MMA] * \frac{1}{t} \qquad \text{[Eq. 1]}$$

where *MG-MMA* is the rate of methanogenesis from MMA (nmol cm^{-3} d^{-1}); a_{CH4} is the radioactive methane produced from methanogenesis (CPM); a_{TIC} is the ^{14}C-TIC produced from

the oxidation of methane (CPM); a_{MMA} the residual ^{14}C-MMA (CPM); RF is the recovery factor; *[MMA]* is the assumed MMA porewater concentrations (nmol cm^{-3}); *t* is the incubation time (d). ^{14}C-CH_4 and ^{14}C-TIC sample activity was corrected by respective abiotic activity determined in dead controls.

Results from the ^{14}C-MMA incubations were also used to estimate the AOM-MMA rates according to Eq. 2,

$$AOM - MMA = \frac{a_{TIC}}{a_{CH_4} + a_{TIC}} * [CH_4] * \frac{1}{t} \quad \text{[Eq. 2]}$$

where *AOM-MMA* is the AOM rate based on methane produced from MMA (nmol $cm^{-3}d^{-1}$); a_{TIC} is the produced ^{14}C-TIC (CPM); a_{CH4} is the residual radioactive methane (CPM); $[CH_4]$ is the sediment methane concentration (nmol cm^{-3}); *t* is the incubation time (d). ^{14}C-TIC activity was corrected by abiotic activity determined by replicate dead controls.

2.7. AOM from ^{14}C-methane

AOM rates from ^{14}C-CH_4 (AOM-CH_4) were determined by injecting radiolabeled ^{14}C-CH_4 (^{14}C-CH_4 dissolved in anoxic MilliQ, injection volume 10 µL, activity 5 KBq, Specific activity 1.85−2.22 GBq $mmol^{-1}$) directly into a separate small whole round core from each station at 1-cm intervals, similar to sections 2.5 and 2.6. Incubations were stopped after ~24 hours and stored at room temperature until further processing, similar to section 2.6. Sediments were then analyzed in the laboratory using oven combustion (Treude et al., 2005) and acidification/shaking (Joye et al., 2004). The radioactivity captured after the headspace combustion and acidification and shaking analysis were determined by liquid scintillation counting. AOM-CH_4 rates were calculated according to Eq. 2.

2.8. Metabolic rate constants for MG-MMA, AOM-MMA and AOM-CH_4

Experimental data determined by sect. 2.6 and 2.7 were used to calculate metabolic rate constants (*k)* to compare relative turnover of MMA and CH_4. We define the rate constants as the metabolic products divided by the sum of the metabolic reactants and products, divided by the incubation time (Krause et al. (2023)).

2.9. Molecular analysis

2.9.1. DNA extraction from sediment

DNA was extracted from approximately 25-30 mg of sediment collected from all sediment intervals in the top ~20 cm of the solid phase push cores from all stations (see above section 2.2) using the PowerSoil DNA Extraction Kit (Qiagen) according to the manufacturer's instructions with the following modifications. Bead tubes were beadbeated for 45 sec at 5.5 m/sec. Samples were eluted first with 50 µL of elution buffer (Solution C6) followed by and additional 25µl of elution buffer for a total of 75uL elution volume.

2.9.2. 16S rRNA gene sequencing (Illumina MiSeq)

The V4-V5 region of the 16S rRNA gene was amplified using archaeal/bacterial primers with Illumina (San Diego, CA, USA) adapters on 5' end (515F 5'-TCGTCGGCAGCGTCAGATGTGTATAAGAGACAG-GTGYCAGCMGCCGCGGTAA-3'and 926R 5'-GTCTCGTGGGCTCGGAGATGTGTATAAGAGACAG-CCGYCAATTYMTTTRAGTTT-3'). PCR reaction mix was set up in duplicate for each sample with Q5 Hot Start High-Fidelity 2x Master Mix (New England Biolabs, Ipswich, MA, USA) in a 15 µL reaction volume according to manufacturer's directions with annealing conditions of 54°C for 30 cycles. Duplicate PCR samples were then pooled and barcoded with Illumina Nextera XT index 2 primers that include unique 8-bp barcodes (P5 5'-AATGATACGGCGACCACCGAGATCTACAC-XXXXXXXX-TCGTCGGCAGCGTC-3' and

P7 5'-CAAGCAGAAGACGGCATACGAGAT-XXXXXXXX-GTCTCGTGGGCTCGG-3'). Amplification with barcoded primers used Q5 Hot Start PCR mixture but used 2.5 µL of product in 25 µL of total reaction volume, annealed at 66°C, and cycled only 10 times. Products were purified using Millipore-Sigma (St. Louis, MO, USA) MultiScreen Plate MSNU03010 with vacuum manifold and quantified using ThermoFisher Scientific (Waltham, MA, USA) QuantIT PicoGreen dsDNA Assay Kit P11496 on the BioRad CFX96 Touch Real-Time PCR Detection System. Barcoded samples were combined in equimolar amounts into single tube and purified with Qiagen PCR Purification Kit 28104 before submission to Laragen (Culver City, CA) for 250 bp paired end sequencing on Illumina's MiSeq platform the addition of 15-20% PhiX.

2.9.3 Analysis of microbial community distribution and 16S rRNA gene sequence data

Sequence data was processed in DADA2 version 1.18 (Callahan et al., 2016). Adapters were removed using cutadept (Martin, 2011). Raw sequences were trimmed to 260bp for forward reads, and 180 bp for reverse reads based on quality of reads. Reads shorter than 260/180 were removed. Error rate was calculated using DADA2's algorithm. Reads were denoised and merged into Amplicon Sequencing Variants (ASV), requiring a 12bp overlap, and chimeras removed. Taxonomic identification for each representative sequence was assigned with the Silva-138 database (Quast et al., 2012) at 100% identity. The SILVA database had been appended with 1,197 in-house high-quality, methane seep-derived bacterial and archaeal clones. The modified SILVA database is available upon request from the corresponding authors.

To visualize the differences between each horizon at each station, a non-metric multidimensional scaling (NMDS) plot was generated. We used Bray-Curtis dissimilarity matrix to calculate the beta diversity of each sample. Each sediment horizon was plotted as an individual dot. The arrow vectors represent the effect of the geochemical characteristic on the

microbial community. The effect of various measured sediment geochemical parameters and calculated metabolic rate measurements for each horizon was calculated with the envfit function (vegan package, Oksanen et al., 2013) and plotted as arrows. The length of the arrow corresponds to the significance (all $p < 0.05$)

3. Results

3.1. Geochemical trends across the transect

3.1.1 Total organic carbon and nitrogen

Fig. 2 B, H, N, and T show the total organic carbon (TOC) and total organic nitrogen (TON) (wt %) and the C/N (based on the ratio of TOC/TON) ratio in the sediment across the sampled salinity gradient. At stations BL and BH, the TOC profiles varied between 1.4% - 4.4% with the highest TOC near the sediment-water interface (Fig. 2B and H). Note at BH, below 11.5 cm TOC decreased < 0.5%. At the M station, TOC was lower than at stations BL and BH, but generally increased with increasing sediment depth reaching 3.9% at 14.5-15.5 cm (Fig. 2N). The HP had the highest TOC in the top 1.5 cm (max 5.4%). Below 1.5 cm, TOC sharply decreased to <0.5% (Fig. 2T).

Generally, TON profiles followed the shape of the TOC profiles at all stations. At BL, TON was between 0.12% and 0.26% (Fig. 2B). At the BH station, TON was between 0.03% and 0.31% (Fig. 2H). At the M station, TON was between 0.04% and 0.21% (Fig. N). At the HP, TON was between 0.02% and 0.38% (Fig. 2T)

At the BL station, the C/N ratio varied between 12 and 18 with the highest C/N within the top 5.5 cm (Fig. 2B). The C/N ratio at the BH station was between 11 and 17 with the highest C/N below 8.5 cm (Fig. 2H). The C/N ratio at the M station increased with sediment depth varying between 11 and 18 (Fig. 2N). The HP station had the highest C/N ratios of all stations, ranging between 13 and 28 with two peaks between 2.5 and 4.5cm and at 10.5-11.5 cm (Fig. 2T).

3.1.2. Salinity and sulfate concentrations

Fig. 2 D, J, P, and V depict the porewater salinity and sulfate concentrations along the sampled salinity gradient. Refractometer measurements of the overlying surface water in the field during low tide showed a natural salinity gradient with fresher and brackish conditions in the northern portion and more saline/hypersaline in the southern portions of the CSMR (Fig. 1). Different to the concentrations found in the overlying surface water, porewater salinity and sulfate increased with sediment depth at both the BL and the BH station. However, max concentrations were lower at BH (47 PSU and 39 mM sulfate) than at BL (73 PSU and 62 mM sulfate) (Fig. 2 D and J). Despite the M station's proximity to the Pacific Ocean and overlying water salinity resembling marine salinities, porewater salinity and sulfate concentrations at the M station decreased from 40 to 22 PSU and from 30 to 9 mM, respectively, with increasing sediment depth (Fig. 2P). The salinity of the overlying water at the HP exceeded all other stations by one order of magnitude (max 135 PSU), classifying it as hypersaline. The porewater salinity and sulfate concentrations at the HP were the highest at the surface (139 PSU and 91 mM, respectively) but decreased with increasing sediment depth (58 PSU and 30 mM, respectively) (Fig. 2V).

3.1.3. Sediment methane concentrations

At the BL station, methane concentration ranged between 7.6 and 16 µM throughout the core without a clear pattern (Fig. 2F). At the BH station, methane was slightly higher in the top 3.5 cm (max 28 µM). Below 3.5 cm, methane concentrations varied with depth ranging between 7.6 and 21 µM (Fig. 2L). Methane concentrations at the M station were lowest in the top 6.5 cm (7 to 16 µM). Below 6.5 cm, methane steeply increased, reaching 55-665 µM between 6.5 and 19.5 cm, which was the highest methane concentration measured across the salinity gradient (Fig. 2R). The steep increase in methane concentration indicates the shallow end of the SMTZ.

However, the sulfate concentration was still > 9 mM at these depths, suggesting that the actual transition zone is located much deeper. Methane concentrations at the HP station peaked at 11.5-12.5 cm reaching as high as 17.5 µM, otherwise methane was between 6 µM and 15 µM without a pattern (Fig. 2X).

3.1.4. Substrate availability for methanogenesis

Porewater concentrations of carbon substrates known to support methanogenesis were determined by NMR. Mono-methylamine was detected in the 0-1.5 cm interval at the BL and HP stations but was below quantification limits (10 µM). Otherwise, mono- methylamine were below the detection limit (< 3 µM) at all other sediment intervals and stations. Methanol was detected below quantification (< 10 µM) within the 9.5-10.5 cm intervals at BL and BH stations and the 14.5-15.5 cm intervals at the M and HP stations. Otherwise, methanol was below detection (<3 µM) at all other sediment intervals across all stations. Acetate was present at quantifiable amounts in certain depth intervals at stations BL (9.5 -10.5 cm), at BH (0-1.5 cm), and at M (14.5-15.5 cm) reaching 61, 45, 72 µM, respectively. Acetate was also detected but below quantification (<10 µM) at stations BH (9.5-10.5 cm) and at HP (9.5-10.5 and 14.5-15.5 cm). Otherwise, acetate was below detection (<3 µM) at all other depth intervals across all stations.

3.1.5. Total sulfide and iron (II) concentrations

Porewater sulfide (H_2S, HS^-, S^{2-}) concentrations were consistently low throughout the sediment core at BL and BH, ranging between 0.8 and 6 µM. In contrast, porewater iron (II) concentrations generally increased with increasing sediment depth at BL and BH reaching 1219 µM and 1116 µM, respectively (Fig. 2C and I). Note iron (II) concentrations at BH decreased from 1116 µM at 10.5 – 11.5 cm to 63 µM at 15.5-16.5 cm before again increasing to 453µM

and the bottom of the core (Fig. 2I). Porewater sulfide concentrations were higher at the M station than at the BL and BH stations with peaks at 0-1.5 cm (22 µM), between 6.5 and 10.5 cm (28 µM), and between 11.5 and 16.5 cm (86 µM). Porewater sulfide concentrations at all other depths were low ranging between 1 to 18 µM (Fig. 2O). Despite having slightly higher sulfide concentrations at the M station, porewater iron (II) concentrations were also high, generally increasing with increasing sediment depth reaching 1661 µM towards the bottom of the sediment core. The HP station showed an inverse relationship between sulfide and iron (II). The highest porewater sulfide concentrations (max 84 µM) were detected at 0-1.5 cm. Below 1.5 cm, sulfide decreased to 7 µM at 4.5-5.5 cm before broadly peaking between 5.5 and 8.8 cm (max 38 µM). Two smaller peaks between 12.5 and 14.5 cm and between 16.5 and 20.5 cm, reached 6 µM and 17 µM, respectively. Iron (II) concentrations varied without trend ranging between 6 µM and 80 µM (Fig. 2U).

3.2. Sulfate reduction from ^{35}S-sulfate and AOM from ^{14}C-CH_4

Fig. 2D, J, P and V show ex-situ rates of sulfate reduction determined from ^{35}S-sulfate incubations across the salinity gradient. At the BL and HP stations sulfate reduction rates were the highest at 0-1 cm, reaching 409 and 2506 nmol cm^{-3} d^{-1}, respectively (Fig. 2D and V). Whereas rates at 0-1 cm at the BH and M stations were considerably lower (11 and 1.5 nmol cm^{-3} d^{-1}) (Fig. 2J and P). The rates at the BH and M stations were highest at slightly deeper sediment intervals (at 1-2 cm and at 3-4 cm, respectively), reaching 1615 and 290 nmol cm^{-3} d^{-1}. Below the most active sulfate reduction zones at the BL, BH and HP stations, rates decreased with increasing sediment depth to either below detection (i.e., below the control levels) or reaching as low as 4, 0.8, and 10 nmol cm^{-3} d^{-1}, respectively. However, at the M station, below 4 cm rates

decreased with increasing sediment depth where it was below detection at 9-10cm (Fig. 2P). Below 10 cm rates broadly peaked with the highest rates at 15-16 cm (227 nmol cm^{-3} d^{-1}).

Fig. 2E, K, Q, and W show the rates of AOM determined from ^{14}C-CH_4 incubations across the transect (AOM-CH_4). At the BL station, AOM-CH_4 rates were low in the top 14 cm ranging between 0.03 and 0.12 nmol cm^{-3} d^{-1} and below detection (i.e., below the control level) below 14 cm (Fig. 2E). At the BH station AOM-CH_4 rates varied between below detection and 0.66 nmol cm^{-3} d^{-1} at 1-2 cm (Fig. 2K). At the M station, AOM-CH_4 was either low or absent within the top 6 cm (max 0.9 nmol cm^{-3} d^{-1}) but then steeply increased reaching a maximum at 12-13 cm (19.4 nmol cm^{-3} d^{-1}) followed by a gradual decreased to 1.3 nmol cm^{-3} d^{-1} at 17-18 cm (Fig. 2Q). At the HP station, AOM-CH_4 rates in the top 7.5 cm were below detection. This zone of high AOM activity coincided with a steep change in methane concentration (Fig. 2R). Below 7.5 cm, AOM-CH_4 peaked between 8.5 and 12.5 cm and between 13.5 and 17.5 cm (0.3 and 0.75 nmol cm^{-3} d^{-1}, respectively) (Fig. 2W).

3.3. Methanogenesis and AOM from ^{14}C-MMA

3.3.1. ^{14}C-MMA recovery factor (RF)

RF values determined in sediment from BL, BH and M stations (see Sect. 2.6.) were 0.66, 0.62, and 0.57, respectively, and were used to correct MG-MMA rates at each station.

3.3.2. MG-MMA and AOM-MMA

Fig. 2 E, K, Q, and W, show the ex-situ rates of methanogenesis from mono-methylamine (MG-MMA) and AOM (AOM-MMA) determined in ^{14}C-MMA incubations. Note that MG-MMA rates are only rough estimates assuming a natural MMA concentration of 3 µM, the detection limits of the method, because natural porewater MMA concentrations were either below detection or below quantification (see Sect. 3.1.4.). At BL, MG-MMA varied between 2.1

and 1 nmol cm^{-3} d^{-1} in the top 6.5 cm (Fig. 2E). Between 7 and 19 cm, rates sharply decreased below where they remained between 0.14 and 0.36 nmol cm^{-3} d^{-1} without trend. At BH, MG-MMA rates gradually decreased between 0 and 7 cm from max 3.8 to 0.14 nmol cm^{-3} d^{-1} (Fig. 2K). Below 7 cm, rates were mostly stable around 0.2 nmol cm^{-3} d^{-1}, except at 11-12 cm, where the rate was below detection, i.e. below the control level. At the M station, MG-MMA rates were overall much lower compared to the BL and BH stations (Fig. 2Q). The highest rate was detected at the sediment surface (0-1 cm, 2.7 nmol cm^{-3} d^{-1}) and rates then decreased to <1 nmol cm^{-3} d^{-1} in the remaining core without any trend. At the HP station, MG-MMA rates were the lowest (Fig. 2W). Two peaks were detected between 0 and 3.5 cm and at 4.5-5.5 cm (0.82 and 0.35 nmol cm^{-3} d^{-1}, respectively). Below 5.5 cm rates were ranged between 0.08 and 0.3 nmol cm^{-3} d^{-1}.

At the BL station AOM-MMA rates, i.e., AOM rates estimated based on the ^{14}C-TIC produced during ^{14}C-MMA incubations, varied between 2.6 and 5.5 nmol cm^{-3} d^{-1} in the top 11 cm, which are two orders of magnitude higher than the AOM-CH_4 at this station (Fig. 2E). Below 11 cm, two peaks were detected at 11-12 cm and between 13 and 19 cm, reaching 7 and 9.5 nmol cm^{-3} d^{-1}, respectively. At BH, AOM-MMA rates were higher than AOM-CH_4 and detected in more sediment intervals with the highest in the top 3 cm (max 16 nmol cm^{-3} d^{-1}) (Fig. 2K). Below 3 cm, rates varied between below detection and 6 nmol cm^{-3} d^{-1}. At the M station, AOM-MMA rates were low (max 3.2 nmol cm^{-3} d^{-1}) in the top 6 cm, but still an order of magnitude higher than the AOM-CH_4 (Fig. 2Q). Rates then increased (max 45.2 nmol cm^{-3} d^{-1}) between 6 and 11 cm, similar to the AOM-CH_4 rates. Below 11 cm, the AOM-MMA rates were below detection. At the HP station AOM-MMA rates varied with increasing sediment depth ranging between 2 and 6 nmol cm^{-3} d^{-1} without trend (Fig. 2W). Note AOM-MMA rates were

detected in the top 5 cm where AOM-CH_4 was not. Also note AOM-MMA was below the detection between 5.5 and 7.5 and between 8.5 and 11.5 cm (where AOM-CH_4 was detected).

3.4. Metabolic rate constants

Metabolic rate constants (k) were plotted to allow for a more direct comparison between the turnover of different ^{14}C radiotracer species. At BL, k for AOM-CH_4 was < 0.1 d^{-1} throughout the sediment core (Fig. 2F), while k for MG-MMA was the highest between 0 and 7 cm (max 0.72 d^{-1}). The k for AOM-MMA was high throughout the sediment core and only slightly increased with sediment depth from 0.5 d^{-1} at the surface to 0.9 d^{-1} at the bottom of the sediment core.

The profiles of the three different rate constants looked very similar at BH station when compared to BL. The k for AOM-CH_4 was constantly low at < 0.1 d^{-1} throughout the sediment core (Fig. 2L). Note at some sediment intervals AOM-CH_4 rates were not detected and thus rate constants are reported as zero. The k for MG-MMA was high at the surface (1.2 d^{-1} at 0-1cm) and decreased to 0.3 d^{-1} at 6-7 cm. Below 7 cm, k varied slightly between 0.02 and 0.08 d^{-1}. The l for AOM-MMA was high throughout the core and varied only slightly with sediment depth between 0.5 d^{-1} and 0.8 d^{-1}. Note that also here some k were zero where AOM-MMA was not detected.

At the M station, k for AOM-CH_4 was zero at 0-1 cm but increased from 0.05 d^{-1} at 1-2 cm to 0.30 d^{-1} at 4-5 cm. Below 5 cm, k varied between 0.07 d^{-1} and 0.3 d^{-1} (Fig. R). The k of MG-MMA showed similar patterns to BH, i.e., gradually decreasing with increasing sediment depth from 0.92 d^{-1} at 0-1cm to 0.054 d^{-1} 16-17cm). The k of AOM-MMA ranged between 0.33 d^{-1} and 0.64 d^{-1} in the top 11 cm. Below 11 cm, AOM-MMA rates were not detected thus k was zero at these depths.

At HP, k for AOM-CH_4 ranged between 0.01 d^{-1} and 0.16 d^{-1} in the 7-11 cm and 13-17 cm sections (Fig. 2X). Otherwise, AOM-CH_4 rates were not detected thus k is zero for those depths. The k of MG-MMA ranged between 0.04 d^{-1} and 0.27 d^{-1} with a small peak at 2-3 cm. The k of AOM-MMA, ranged between 0.56 d^{-1} and 0.8 d^{-1} in the top 5.5 cm. At 7.5-8.5 cm, and between 11.5 and 17.5 cm k was consistently around 0.95 d^{-1}. In between these positive values, k was zero, because no activity was detected.

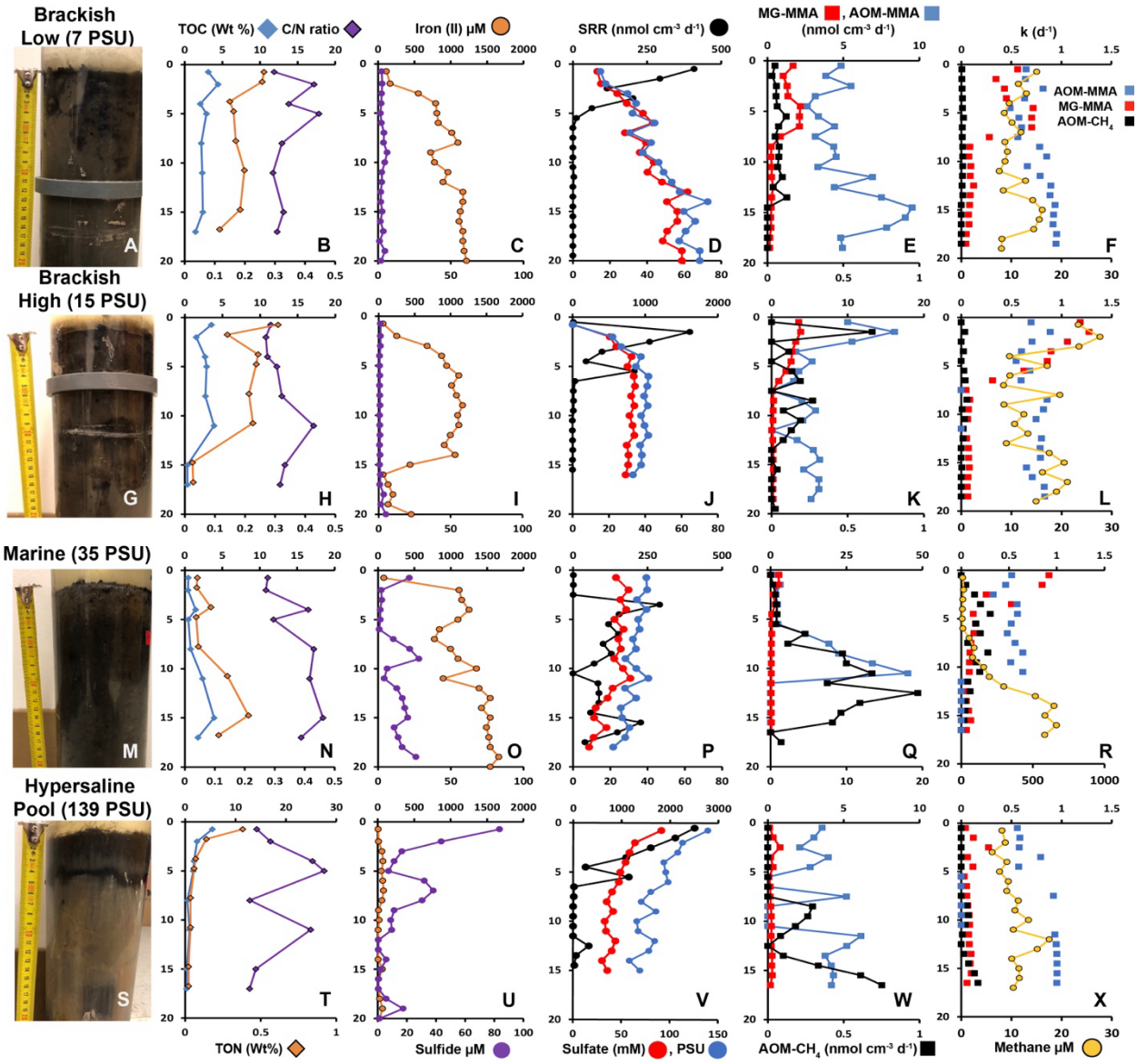

Figure 2. Depth profiles of (bio)geochemical parameters determined in sediment cores collected from the four different stations in the Carpinteria Salt Marsh Reserve. Left Panel: Photos of the sediment cores collected (with scale) from the Brackish Low (**A**), Brackish High (**G**), Marine (**M**), and Hypersaline (**S**) stations. **B**, **H**, **N**, and **T**: TOC, TON and C/N ratio. **C**, **I**, **O**, and **U**: Porewater sulfide and iron (II). **D**, **J**, **P**, and **V**: ex-situ sulfate reduction rates (SRR), porewater sulfate, and porewater salinity. **E**, **K**, **Q**, and **W**: AOM rates derived from ^{14}C-mono-methylamine (AOM-MMA) incubations, methanogenesis rates from ^{14}C-mono-methylamine (MG-MMA) incubations, and AOM directly derived from ^{14}C-methane (AOM-CH_4) incubations. **F**, **L**, **R**, and **X**: Metabolic rate constants (k) of AOM-MMA, MG-MMA, AOM-CH_4 incubations and sediment methane concentration. Note scale changes on the x-axis.

3.5. Methanogenesis batch incubations

Fig. 3 shows results from the in vitro time-series incubation of methanogenesis with natural sediments collected from each station (see details in section 2.3.). Methane in the headspace of vials from all stations and depth intervals did not show any linear increase over the course of 530 hours. At the BL, BH, and HP stations, methane remained very low with small oscillations ranging between 40 and 258 ppmv (Fig. 3A, B, and D).

In the 0-5 cm depth interval of the M station, methane showed a similar pattern as the other stations, ranging from 66 to 115 ppmv (Fig. 3C). However, the 5-14 cm (239 to 356 ppmv) and 14-19 cm (366 to 508 ppmv) interval of the M station showed elevated methane, which peaked at 312 hrs after which methane decreased again.

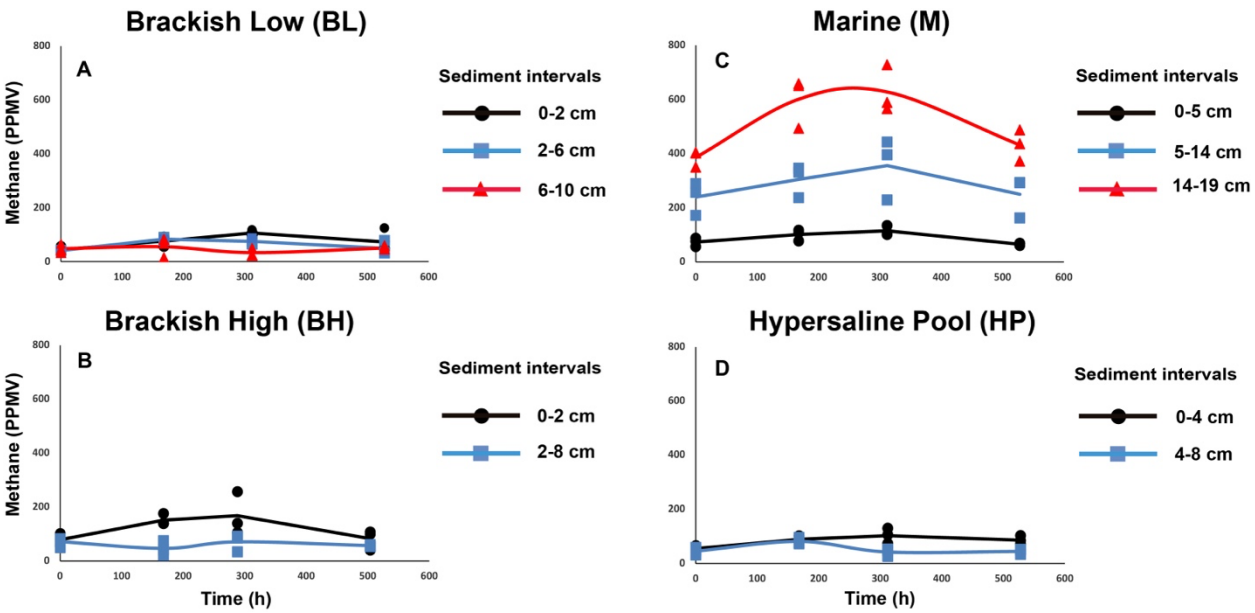

Figure 3. Methane development during methanogenesis batch incubations with sediments from discrete layers over time; (**A**) Brackish Low, (**B**) Brackish High, (**C**) Marine, and (**D**) Hypersaline Pool.

3.6 Spatial microbial community patterns

Differences in microbial community structure (all Prokaryotes) were observed between the 4 stations, (Fig. 4). NMDS results showed that the communities of each horizon from the BL and BH grouped closer together, indicating similar beta diversity. Interestingly, microbial

community structure at the M station groups was significantly split into two distinct groups. While the microbial community structure at the HP station was the least similar to the rest of the stations. We found that MG-MMA rates are significantly correlated (P-value = 0.016) with the microbial communities in the BL and BH stations. AOM-CH_4 and AOM-MMA rates are significantly correlated with microbial communities in the M station (P-values = 0.001 and 0.007, respectively). Sulfate reduction was significantly correlated with the microbial community in the HP station (P-value = 0.002).

We found that high salinity and sulfate were significantly (P-value = 0.001) correlated with the microbial community in the HP station compared to the other stations, while methane was significantly correlated (P-value = 0.002) with microbial community in the M station. Higher sulfide was significantly correlated with some of the microbial communities at the M and HP stations, while the BL and BH stations were significantly correlated with higher iron (II) (P-value = 0.001).

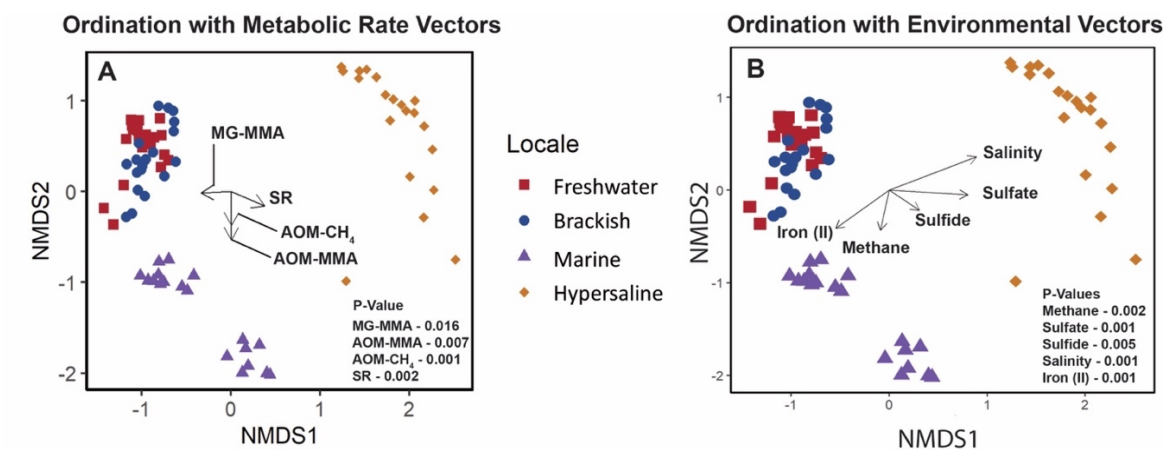

Figure 4. NMDS plots showing microbial community structure (all Prokaryotes) of each station relative to each other and correlations of microbial communities to metabolic rates (**A**) and geochemical parameters (**B**).

3.7 Relative abundance of archaeal and bacterial communities

3.7.1 Methanogenic and methanotrophic signals

Fig. 5 shows amplicon sequence variants (ASVs) of the most abundant archaeal families belonging to methanogenic (*Methanosarcinaceae*, *Methanosaetaceae, Methanoregulaceae,* and *Methanonatronarchaeacea*) and anaerobic methanotrophic archaea (ANME 2a-c), that were detected in the sediment across the salinity gradient. All methanogenic archaeal groups that were detected in the present study are found in anoxic sediment. The *Methanosarcinaceae* family are found in anoxic sediment in freshwater and marine environments and the *Methanosaetaceae* family are found in freshwater sediment (Liu and Whitman, 2008). *Methanoregulaceae* have been found in acidic peat bogs, anaerobic reactors, oil fields, rice paddy soil, a mud volcano, and in a freshwater lake (Oren, 2014). *Methanonatronarchaeacea* are found in hypersaline environments (Sorokin et al., 2018). The methanogens within the *Methanosarcinaceae* family are able to use acetate, methylated substrates, and H_2/CO_2 to produce methane while methanogens within the *Methanosaetaceae* family are obligate acetoclastic methanogens (Liu and Whitman, 2008). The methanogens within the *Methanoregulaceae* family use H_2/CO_2 to produce methane (Oren, 2014). The methanogens within the *Methanonatronarchaeacea* family use methylated substrates and H_2/CO_2 to produce methane (Sorokin et al., 2018). ANME 2a and b are commonly found in marine and salt marsh (ANME 2a) sediment, whereas, ANME 2c has been found in freshwater, brackish and marine sediment; all of these groups of ANME are partnered with sulfate-reducing bacteria to couple methane oxidation with sulfate (Timmers et al., 2017; Knittel and Boetius, 2009).

The BL station generally had the lowest abundance of archaeal families (Fig. 5A). At BL, only one methanogenic family was detected at low abundance (0.35%) at 4-5 cm, which belonged to *Methanosarcinaceae*. At BH, low ASV abundances of *Methanosarcinaceae* were found in deeper sediment intervals at 13.5-14.5 cm and between 15.5 and 17.5 cm (0.26, 0.44

and 0.46%, respectively) (Fig. 5B). ASVs belonging to anerobic methanotrophic (ANME) archaea families were not detected in the BL and BH stations, which coincides with low AOM rates at these stations (Fig. 2E and K). At the M station, both methanogenic and methanotrophic archaea were much more prevalent than at any of the other stations (Fig. 5C). At the M station, where some of the highest AOM rates were detected (Fig. 2Q) ANME-2a-2b dominated over the methanogenic archaea, reaching 6.5 and 5.3% at 4-5 and 11.5-12.5 cm, respectively. ANME-2c ASVs were also detected at low relative abundance at 4.5-5.5 and 12.5-13.5 cm reaching 0.48 and 0.73%, respectively. At the M station ASVs belonging to one group of methanogens, *Methanosarcinaceae,* was detected at 7.5-8.5 cm (0.45%) and coincides with low rates of MG-MMA (Fig. 2Q). While at 12.5-13.5 cm, more ASVs belonging methanogenic archaeal families of *Methanosarcinaceae*, *Methanosaetaceae* and *Methanoregulaceae* were detected, reaching 0.41, 0.85, and 0.53%, respectively (Fig. 5C). Note these methanogenic ASV's were found alongside the ANME 2a-2b and 2c archaeal ASVs at this depth interval. Below 12.5 cm, methanotrophic archaea were not detected, but a higher percentage of the ASV belonged to *Methanosarcinaceae*, *Methanosaetaceae*, *and Methanoregulaceae* reaching 7.8, 2.3, and 0.95%, respectively (Fig. 5C).

Archaeal family ASVs were highest at the HP station. ASVs belonging to ANME 2a-2b, and 2c were detected in the top 2.5 cm, reaching 2.8 and 2.1% at 0-1.5 cm, respectively. This coincides with detectable AOM-MMA rates but not with AOM-CH_4 rates, which were below detection at these depth intervals (Fig. 2W). Below 2.5 cm, methanotrophic ASVs were not detected (Fig 5D), but AOM rates were detectable (Fig. 2W). Methanogenic ASVs belonging to the family *Methanonatronarchaeacea* were detected in deeper sediment intervals between 4.5 and 8.5 cm and again between 15.5 and 20.5 cm reaching as high as 1.9% and 2.1%,

respectively. *Methanosarcinaceae* ASV's were also detected at 17.5 – 18.5 cm. Figure 5A-D also shows that the methanogenic and methanotrophic archaeal groups are accompanied by other families which are reported in Suppl. Fig. S1.

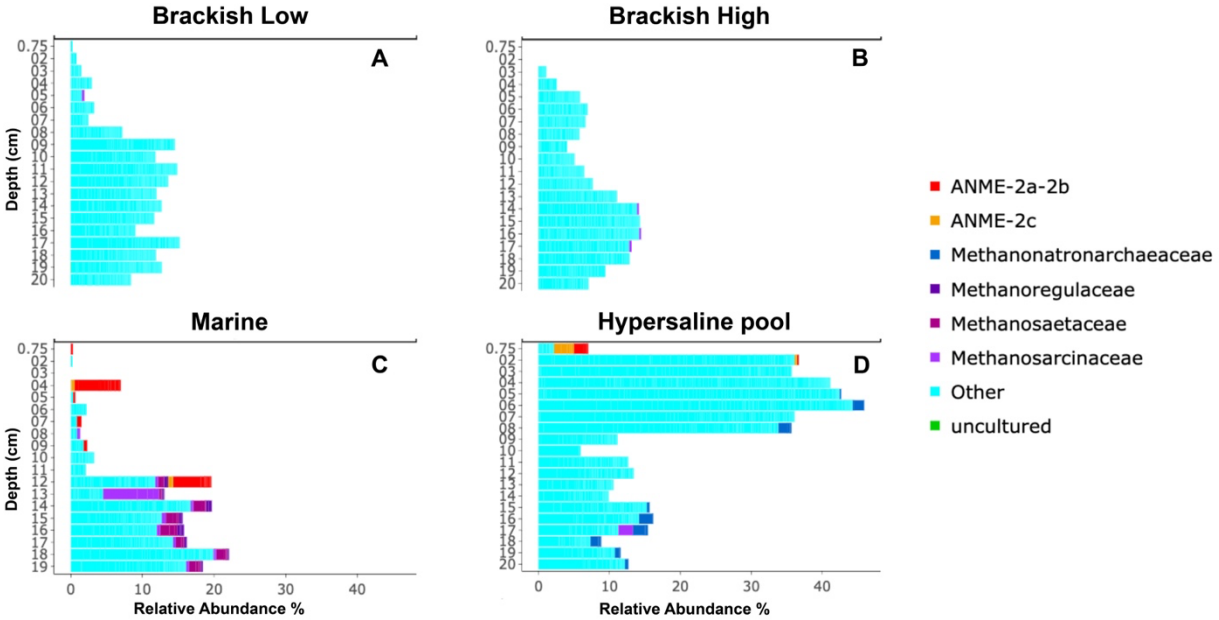

Figure 5. Relative abundances of methanogenic and and anaerobic methanotrophic archaea along the CSMR transect.

3.7.2 Distribution of Desulfobacterota phylum

Figure 6A-D shows the ASVs belonging to orders of sulfate-reducing bacteria within the Desulfobacterota phylum that were detected in the sediment across the CSMR transect. Members within the Desulfobacterota phylum are the dominant sulfate-reducing organisms that are found in surface sediments in marine and freshwater environments (Waite et al., 2020; Diao et al., 2023). It is worth noting that many members within this phylum (Geobacterales, Geopsychrobacteraceae, Geothermobacteraceae, and Desulfuromondaceaae) are able to utilize oxidized metals such as iron for their metabolisms (Waite et al., 2020; Holmes et al., 2004; Young, 2003). Furthermore, it has been shown that orders within Desulfobacterota (Desulfobacterales, Desulfobulbales, Desulfovibrionales) have members that are able to do iron reduction in addition to sulfate reduction (Reyes et al., 2017; Park et al., 2008)

At the BL station, ASV's belonging to Desulfobulbales order were detected in the top 9.5 cm (where high sulfate reduction rates and porewater iron (II) were detected (Fig. 2C and D)) with relative abundances ranging between 1.4 %and 11 %. Whereas ASVs belonging to Desulfobacterales (part of Desulfobacterota 1) with relative abundances between 2.8-6.9 % were detected throughout the sediment core (Fig. 6A). BL was the only station containing ASV's belonging to Desulfuromonadaceae_1 between 4.5-6.5 cm ranging between 1% and 2.5%. Between 15.5 cm and 19.5 cm ASV's belonging to Syntrophobacterales were detected ranging between 1% and 1.4%. Desulfobulbales and Desulfobacterales ASV trends at the BH station were similar to the BL station, however, Desulfobulbales abundances (ranging between 1.5-10%) extended from the surface into deeper sediment intervals down to 12 cm (Fig. 6B). Desulfobacterales' ASV's at the BH station were also higher than at the BL station, ranging between 2.4-11.8%. Stations BL and BH were the only stations with ASV's belonging to Desulfatiglandales ranging between 1% and 4.5%, which were found between approximately 5.5 cm and 20.5 cm. ASV's belonging to Syntrophobacterales were also detected at BH between 4.5 and 13.5 cm and at 14.5-15.5 cm, at 17.5-18.5 cm, and 19.5-20.5 cm, ranging between 1% and 1.8%. At the M station, Desulfobacterales abundances were the highest in the top 11 cm, reaching 26.9% at 8.5-9.5 cm (Fig. 6C), and corresponds with high sulfate reduction rates and porewarter iron (II) (Fig. 2I and J). Below 12 cm, Desulfobacterales abundances declined, ranging between 1.3-4.6%. Desulfobulbales was also detected in the top 11 cm but were lower (4.1%-7.4%) compared to the relative abundance of Desulfobacterales. The M station was the only station containing ASV's belonging to Geopsychrobacteraceae (ranging between 1.3% and 4.3%), Geobacterales (ranging between 1.4% and 4.7%), and Syntrophales (ranging between 1% and 1.4%) in the top 11.5 cm, below 12.5 cm, and below 16.5 cm, respectively. The HP station

had the least amount of ASVs belonging to sulfate-reducing phyla (Fig. 6D), despite having the highest sulfate reduction rates out of all stations (Fig. 2V). However, Desulfobacterales were detected between 0 and 5 cm, at 8.5-9.5 cm and at 10.5-11.5 cm ranging between 1.1-7%. Desulfobulbales ASV's were also detected at 0-1.5 cm, 3.5-4.5 cm, 8.5-9.5 cm and 10.5-11.5 cm with low abundances ranging between 1-2%. One sediment interval at 1.5-2.5 cm had ASV's belonging to Desulfovibrionales at low relative abundance (2%) (Fig. 6D). The HP station was the only station containing ASV's belonging to Geothermobacteraceae between 6.5cm and 13.5 cm and at 19.5-20.5 cm, ranging between 1% and 4.3%, where smaller concentrations of porewater iron (II) were detected (Fig. 2U). ASV's belonging to Syntrophobacterales was also detected in the HP station at 8.5-9.5 cm and between 11.5 and 20.5 cm, ranging between 1.2% and 2.8% (Fig. 6D).

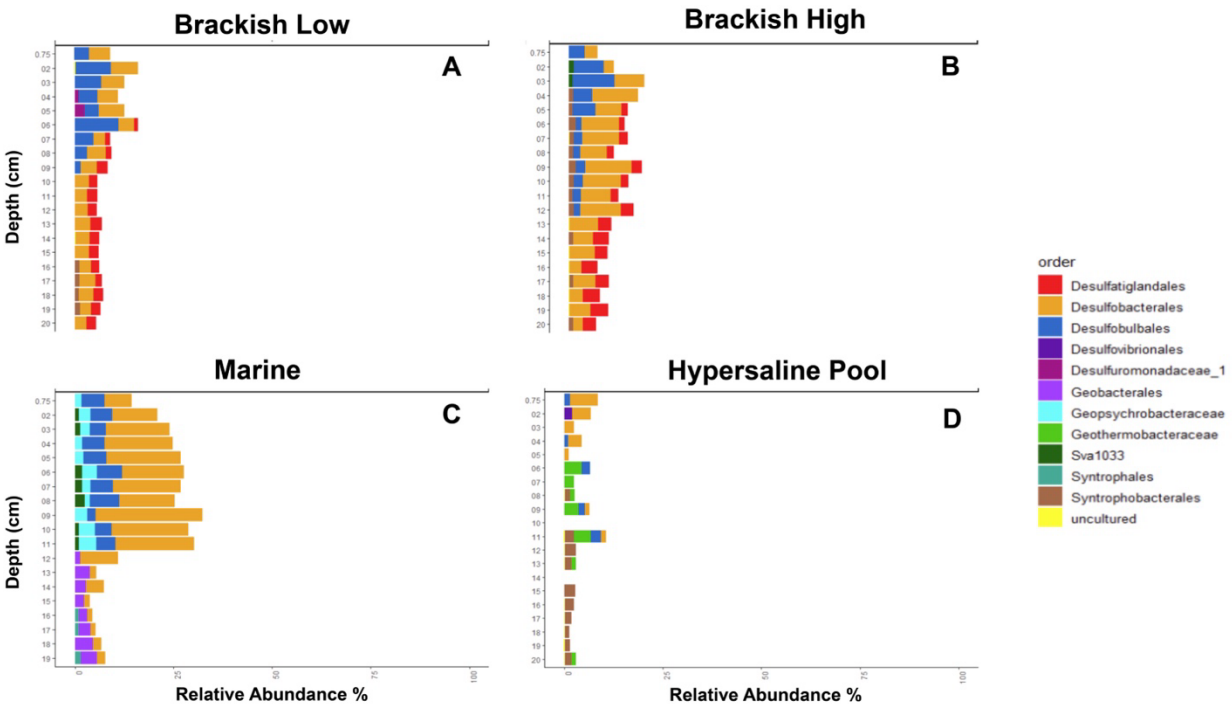

Figure 6. Relative abundances of bacterial orders within the Desulfobacterota phylum.

3.7.3. Dominant bacterial phyla across the salinity gradient

Fig. 7 shows the top 36 bacterial phyla ASVs detected in the sediment across the salinity gradient. Aside from phyla containing bacteria that can perform sulfate/iron reduction, other bacterial phyla seem to be much more dominant in the CSMR sediment across the salinity gradient. Bacteria phylum ASVs belonging to Proteobacteria are present throughout the sediment at all stations but more prevalent in the top 10.5- 11.5 cm at BL, BH and M stations (35%-26%, and more evenly dominant throughout the sediment at station 4 (5.5%-45%). At the BL and BH stations bacterial phylum ASVs belonging to Planctomycetota are more prevalent in sediment intervals below 7 cm, reaching as high as 29% and 24%, respectively. At the M station ASVs belonging to Planctomycetota are present throughout the sediment but are lower than at the BL and BH stations, reaching 12%.

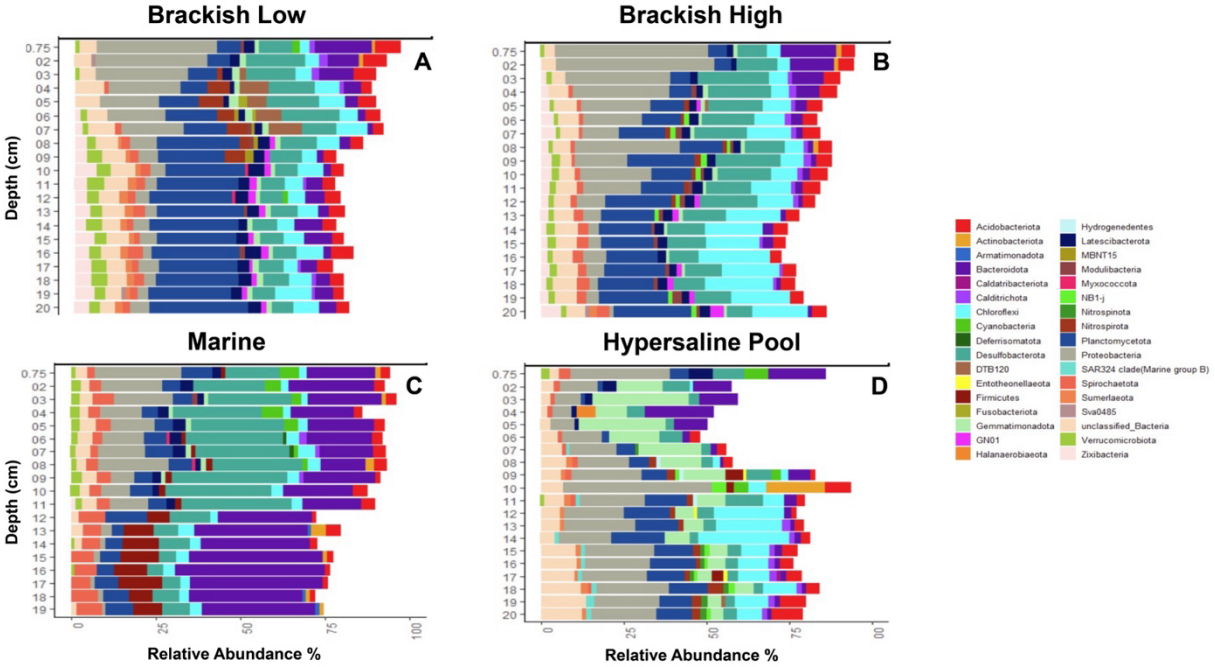

Figure 7. Relative abundances of the top 36 bacteria phylum detected in the sediment of the CSMR transect.

4. Discussion (Preliminary interpretations)

4.1 Spatial evidence of cryptic methane cycling

The aim of this study was to find evidence of cryptic methane cycling across the land-ocean transect in the CSMR, by presenting geochemical evidence along with concurrent activity of methanogenesis linked to mono-methylamine (in the following termed 'methylotrophic methanogenesis'), sulfate reduction, and AOM from radiotracer incubations (^{14}C-MMA, ^{35}S-SO_4^{-2}, and ^{14}C-CH_4, respectively). Based on our ^{14}C-MMA incubations, methylotrophic methanogenesis was supposedly active at all stations and throughout the sampled intervals. Radiotracer experiments further suggested that methylotrophic methanogenesis overlapped with AOM in the 0-14, 1-19, 1-18, and 7-17 cm section at the BL, BH, M, and HP stations, respectively (Fig. 2E, K, Q, and W). These findings indicate that methylotrophic methanogenesis is directly fueling AOM at the investigated stations. Note however, that AOM was below the detection limit in some sediment intervals at the BH and M stations and comparably low (< 1 nmol cm^{-3} d^{-1}) at the BL and BH stations. Sulfate reduction, a process potentially linked to AOM, was found to be active alongside methylotrophic methanogenesis and AOM in the 1-6, 1-16, 0-18 and 13-15 cm sections at the BL, BH, M, and HP stations (Fig. 2D, E, J, K, P, Q, V, and W). Our data suggest that the activity of sulfate reduction and methylotrophic methanogenesis is driven by the availability of organic matter. For example, higher TOC (3.5-4.4%) and TON (0.26-0.31%) were found within the top 2.5 cm at both BL and BH (Fig. 2B and H). These TOC and TON contents were within the range of TOC and TON found in surface sediment in other salt marshes, such as the North Inlet salt marsh South Carolina, USA (1.6-9.4% for TOC; 0.15-0.6% for TON) (Chen et al., 2016)), the low salt marshes of the Finistere region, France (Goslin et al., 2017)), and the salt marshes within the Cádiz Ba, southern Spain (approx. 3% for TOC;

approx. 0.3% for TON) (De Los Santos et al., 2023).The C/N ratios at the BL and BH stations suggest that the organic matter is likely sourced from a mixture of terrestrial plants (C/N > 20) and marine organic matter (C/N between 5 and 8) (Fig. 2B and H) (Meyers, 1994; Xia et al., 2021). Terrestrial plants were found lined against the embankments and submerged within streams at the BL and BH stations which are likely supplying the organic matter detected (Fig. 1). Previous studies have shown that coastal marsh vegetation is an important source of organic carbon into the sediment (Reddy et al., 2022; Bartoli et al., 2021), which can enhance sulfate reduction (Jackson et al., 2014; Kostka et al., 2002) and methanogenesis (Yuan et al., 2014; 2019).

Accordingly, a lower TOC and TON content was detected at the M station (Fig. 2N), potentially explaining lower or undetectable sulfate reduction and methylotrophic methanogenesis activity within the top 10 cm (Fig. 2P and Q). Field and lab observations of the sediment from the M station indicated a larger sediment grain size (sand) in the top 10 cm compared to finer grained silt and muds found at BL and BH. Previous work have shown that permeable sands are sites for enhanced organic matter consumption (Boudreau et al., 2001) because flow into permeable sandy sediment delivers more particulate organic matter (Huettel et al., 1996; Rusch et al., 2001), and oxygen (Booij et al., 1991; Ziebis et al., 1996; Precht et al., 2004), and quickly remove products of degradation (Huettel et al., 1998; Rocha, 1998). This would then ultimately result in sediment intervals near the surface to not be fully anoxic/reduced which is necessary for sulfate reduction and methanogenesis to occur in the sediment at the M station.

Different to Krause and Treude (2021), who found concurrent peaks of methylotrophic methanogenesis and AOM in the top 5 cm at the HP station, overlap of the two processes was

detected only in deeper sediment intervals (> 12 cm, Fig. 2W) at the HP station in the present study. It is worth noting that in the present study sediment from the HP pool was collected approximately one year after and one meter away from the original sampling spot studied in Krause and Treude (2021), suggesting that cryptic methane cycling activity is subject to natural temporal and spatial variation.

Methane concentrations detected within sulfate-rich sediment is likely sourced from methanogenesis via methylotrophic pathways (Oremland and Taylor, 1978; King et al., 1983; Maltby et al., 2016; Reeburgh, 2007), which is further supported by the ^{14}C-methane produced during the ^{14}C-MMA incubations (Fig. 2 E, K, Q, W). Methane concentrations in sediment cores from the BL, BH, and HP station were about an order of magnitude lower (<28 μM) than what has been previously reported from the top 20 cm of sediment at other coastal wetlands, such as within the Arne Peninsular salt marsh, UK (up to 100 μM) (Parkes et al., 2012), the Queen's Creek Tidal Marsh, VA, USA (up to 450 μM, in July) (Bartlett et al., 1987), the Chongming Island of the Yangtze Estuary, East Asia (up to 156 μM) (Li et al., 2021), and Dover Bluff salt marsh, GA, USA (0.3-1.2 mM) (Segarra et al., 2013). Instead, methane profiles at the BL, BH and HP stations, were consistently low between 3 and 28 μM (Fig. 2 F, L, and X). These low methane concentrations could represent the equilibrium between methylotrophic methanogenesis and AOM as part of the cryptic methane cycle in sulfate-reducing sediment (Krause et al., 2023). The observed methane profiles are opposite the classical diffusion-controlled trend where residual methane linearly declines between the SMTZ and the sediment-water interface, which is often seen in coastal wetlands (Segarra et al., 2013; Bartlett et al., 1987; Parkes et al., 2012) and marine environments (Reeburgh, 2007; Bernard, 1979; Tilbrook and Karl, 1995; Iversen and Jørgensen, 1993) including the M station from the present study. Methane profiles at the BL,

BH, M (top 5 cm), and HP stations were more similar to organic-rich surface sediment in the oxygen-deficient Santa Barbara Basin, where the simultaneous production and consumption of methane was also detected (Krause et al., 2023). Note the methane profile in deeper sediment intervals (> 5 cm) at the M station resembled classic methane profiles in deeper anoxic sediments found in marine sediment (Bernard, 1979; Tilbrook and Karl, 1995; Reeburgh, 2007). Another support for the presence of cryptic methane cycling comes from the methanogenesis batch incubations (Fig. 3A, B, C and D), which show no linear buildup of methane in the headspace over ~530 hrs, except in sediment from the 5-14 cm and 14-19 cm layers of the M station. While there are two ways to interpret the lack of methane build up in the batch incubations, i.e., either the absence of methane production or the presence of simultaneous methane production and consumption, our radiotracer data point towards the latter scenario. Together, the radiotracer and batch incubations strongly suggest simultaneous methane production and consumption by the cryptic methane cycle across the salinity transect.

4.2. Spatial geochemical trends and electron acceptors for AOM

Another goal of this study was to compare porewater salinity and electron acceptor availability with metabolic processes (i.e., sulfate reduction and AOM) along the transect. Although the salinity in the overlying water indicated a natural salinity gradient within the CSMR due to freshwater and seawater convergence, the porewater salinity (max 73 and 47 PSU at BL and BH, respectively) and sulfate concentrations (max 62 and 39 mM at BL and BH, respectively) in the brackish stations increased with increasing sediment depth and were considerably higher than expected (Fig 2D and J.). This finding suggests that the sediment hydrology of the CSMR is heavily influenced by seawater infiltration rather than by freshwater sources (i.e., by watersheds located more inland). Alternatively, it may also suggest that the

CSMR was once a hypersaline coastal wetland. The abundance of salt within salt marshes such as the CSMR is largely controlled by tidal infiltration and inundation and by evaporation (Gardner, 2007; Moffett et al., 2010; Li et al., 2023). For the CSMR sediments to have accumulated such high amounts of salts, the area must have had periodic inundation by seawater to deliver the salt, followed by evaporation. It is conceivable that subsurface hydrology and the geomorphology of the CSMR plays a role in the salinization and/or dilution of the salt in the subsurface of the CSMR (Reddy et al., 2022). However, the present study did not determine the direction of seawater penetration/infiltration (vertical or lateral diffusion) but future studies at the CSMR and other coastal wetlands would benefit from such determinations because the seawater delivers sulfate, which is a key electron acceptor for AOM.

Porewater sulfate across the salinity gradient of the CSMR did not reached concentrations below 9 mM, with the exception of the 0-1 cm section at the BH station, where sulfate was 0.15 mM (Fig. 2 D, J, P, V). Non-limiting sulfate concentrations in the sediment at all stations across the salinity gradient support high sulfate reduction activity found in the top 5-10 cm and is strongly correlated with microbial communities in the HP station (Fig. 4A and B) which had the highest sulfate reduction rates (Fig. 2V). Importantly, in depths where sulfate reduction activity overlapped with AOM (e.g., 1-6, 1-10, 1-18, and 13-15 cm sections at the BL, BH, M, and HP stations, respectively), AOM could be coupled to sulfate reduction (while a part of sulfate reduction was likely also linked to organic matter degradation). In addition, the 16S sequencing data detected the presence of bacterial groups capable of sulfate reduction in all layers where there was overlap of sulfate reduction and AOM rates (Fig. 2 and 5) and where ANME groups were also detected (Fig. 5C and D), except at the BL and BH stations where ANME groups were not detected (see section 4.3 for details).The high porewater sulfate concentrations along the

CSMR salinity transect, despite high sulfate reduction activity, suggests that sediment within coastal wetlands like the CSMR are reservoirs of electron acceptors, which are important to buffer methane production by competitive methanogenesis pathways (Kristjansson et al., 1982; Winfrey and Ward, 1983; Lovley and Klug, 1986; Jørgensen, 2000) and support methane consumption by AOM (Knittel and Boetius, 2009).

Porewater iron (II) and sulfide concentrations (Fig. 2 C, I, O, and U) revealed that sediment below the top 2 cm in the CSMR transitioned from a predominantly iron-reducing (high Fe (II), absence of sulfide) environment to a predominantly sulfate-reducing (low Fe (II), presence of sulfide) environment between the BL and the HP stations. Additionally, the microbial community analysis shows a strong correlation between the high iron (II) concentrations and the microbial communities at the BL and BH stations strongly suggesting that there are groups within the microbial communities of the BL and BH stations that are involved in iron cycling (Fig. 4B) (Reddy and Delaune, 2008; Reddy et al., 2022; Lovley, 2006). Our 16S sequencing results the CSMR stations show the presence of Acidobacteriota, Firmicutes, Deferrisomatota, and Sva 0485 phyla which are phyla known to contain groups of iron-reducing bacteria (Fig. 7A, B, C, and D) (Weber et al., 2006). Additionally, the sequencing data also show that in the iron-reducing layers in the BL and BH stations are dominated by orders of bacteria (i.e., Desulfatiglandales, Desulfobacterales, and Desulfobulbales), capable of performing iron reduction and could potentially be contributing to the buildup of iron (II) at these stations without the presence of obligate iron-reducing bacteria (Fig. 6A and B). Similar observations have been made where groups within Desulfobacterales and Desulfobulbales were detected in iron-reducing sediment and potentially actively contributing to iron reduction in the Baltic Sea (Reyes et al., 2017).

At the M and HP stations, porewater sulfide was more abundant than at the BL and BH stations (Fig. 2O and U). The sulfide production is likely attributed to the widespread sulfate reduction activity at both stations, and sulfate reduction coupled to AOM more so at the M station, that was detected from the radiotracer incubations (Fig. 2P and V). This compares well with the microbial community analysis where microbial communities at the M station are correlated with sulfide and AOM rates while the HP station is correlated with sulfate reduction rates and sulfide (Fig. 4A and B). At the M station, porewater sulfide was also accompanied with high porewater iron (II) (Fig. 2O), which coincides with some microbial communities correlated with porewater iron (II) (Fig. 4B). The 16S sequencing data at the M station shows there is a mixture of iron-reducing bacteria (i.e., Acidobacteriota, Firmicutes, Geobacterales, Geopsychrobacteraceae, Geothermobacteraceae, and Desulfuromondaceaae) and sulfate/iron-reducing bacteria (i.e., Desulfobacterales and Desulfobulbales) throughout the sediment (Fig. 6C and 7C). This mixture of microbial groups could potentially be contributing to the large buildup of both iron (II) and sulfide in the sediment at the M station (Fig. 2O). Whereas, at the HP station, sulfate/iron-reducing bacteria (i.e., Desulfobacterales and Desulfobulbales) that were detected near the sediment surface could potentially be responsible for the high sulfate reduction rates and high sulfide concentrations near the sediment surface (Fig. 2 U and V). The sequencing data also detected an iron reducer (i.e., Geothermobacteraceae) and sulfate/iron reducers (i.e., Desulfobacterales and Desulfobulbales) (Fig. 6D) just below the sulfate-reducing layer which potentially is responsible for the small amount of iron (II) buildup (Fig. 2U). The geochemical and molecular data in this study strongly indicate that both iron reduction and sulfate reduction are concurrently active, potentially by groups of iron-reducing and sulfate-reducing bacteria that are present at the M station (Fig 2O and 6C), and to a lesser extent at the HP station (Fig. 2U and

6D). Simultaneous iron and sulfate reduction has been observed in marine (Postma and Jakobsen, 1996), lacustrine (Motelica-Heino et al., 2003) and wetland sediment (Reddy and Delaune, 2008). The detection of simultaneous iron and sulfate reduction activity is interesting since iron reduction is thermodynamically more favorable than sulfate reduction for shared substrates such as hydrogen and acetate (Jørgensen, 2000) and would typically suppress sulfate reduction activity and ban it to deeper sediment intervals (Lovley and Phillips, 1987). However, iron oxides have been shown to persist below sulfate reduction layers in sedimentary environments that receive high inputs of iron-oxides and/or have sediments that have undergone transient diagenesis (Egger et al., 2015). Nevertheless, this study shows that the CSMR sediment appears to be both sulfate and iron rich (Fig. 2C, D, I, J, O, P, U, and V) which support sulfate and iron-reducing communities (Fig. 6 and 7) are in parallel regulators of methane by not only suppressing the methanogens doing competitive methanogenesis pathways but could potentially also supporting the AOM rates (Fig. 2E, K, Q, and W) as part of the cryptic methane cycle .

The importance of finding iron-reducing sediment in the CSMR transect is that although AOM is typically coupled to sulfate reduction in sediment where sulfate is present and all other electron acceptors are depleted, AOM can be coupled to iron-reduction in the presence of iron oxides (Knittel and Boetius, 2009). Iron-dependent AOM and has been shown to occur in marine (Beal et al., 2009; Rooze et al., 2016), brackish (Egger et al., 2015; Egger et al., 2017), and freshwater (Martinez-Cruz et al., 2018; Ettwig et al., 2016), and coastal wetland environments (Segarra et al., 2013; Wallenius et al., 2021; Valenzuela et al., 2019). Iron (III) could be an important electron acceptor for AOM in deeper sediment intervals at the BL, BH, and M stations, where iron (II) is high (Fig. 2C, P and I). However, ANME families that are known to be able to do iron-dependent AOM were not detected in the BL and BH stations (Fig. 5A and B). At the M

station, however, ASVs belonging to ANME 2a and c (Fig. 5C), which have recently been proposed to perform iron-dependent AOM in marine sediments (Scheller et al., 2016; Aromokeye et al., 2020) were detected. Although the present study did not directly test for the coupling of iron to AOM, at a minimum our study shows a buildup of iron (II) in the sediment at BL, BH and M stations, indicating that iron (III) could potentially be an important electron acceptor in general and potentially for AOM. However, more work is needed to connect the role of iron to the cryptic methane cycle in the CSMR.

4.3. Archaeal methanogen and methanotroph communities

Another goal of this study was to elucidate the archaea responsible for methanogenesis and AOM across the CSMR transect and to investigate whether they overlap in occurrence, providing more evidence for cryptic methane cycling in the CSMR. At the BL and BH stations, MG-MMA rates were strongly correlated with microbial communities at these stations (Fig. 4A). ASVs belonging to *Methanosarcinaceae*, a known methanogen capable of producing methane from non-competitive substrates (Boone et al., 2015), was detected at low abundances at the BL and BH stations (Fig. 5A and B) in sediment intervals where we detected methylotrophic methanogenesis (Fig. 2E and K). However, no families belonging to ANME were detected from the 16S sequencing (Fig. 5A and B). The lack of genetic evidence of ANME coincides with the very low (<< 1 nmol cm^{-3} d^{-1}) or below detection AOM rates at these stations (Fig. 2E and K) so it is possible that the genetic material belonging to ANMEs were too low to be detected by the methods.

At the M station, relative ASV abundances of ANME 2a-c dominated over methanogen ASVs in shallower sediment intervals (< 9 cm) (Fig. 5C) and are likely responsible for the detected AOM-CH_4 activity, keeping methane concentrations low (Fig 2Q and R). ASVs

belonging to ANME 2a-2c were detected at 12.5-13.5 cm which could be responsible for the dramatic increase in AOM rates and decline in methane concentrations above and below this section (Fig. 2Q and R). In the same section (12.5-13.5 cm) ASVs belonging to *Methanosarcinaceae, Methanoregulaceae*, and *Methanosaetaceae* were found, suggesting that methanogens, capable of non-competitive methanogenesis (Boone et al., 2015), and ANME are coexisting in sulfate-reducing sediment at the M station. ASVs belonging to ANMEs were not detected between 13.5 and 19.5 cm despite detecting higher AOM rates (Fig. 2Q). Instead ASVs belonging to *Methanosarcinaceae*, *Methanoregulaceae*, and *Methanosaetaceae* extended into deeper horizons between 13.5 and 19.5 cm, which could be linked to the higher methane concentrations found in these depths (Fig. 2R) as well as the higher levels of methane temporarily produced in methanogenesis batch incubations with deeper sections (Fig. 3C).

Interestingly, ANME 2a-2c families were detected in the top 2.5 cm at the HP station; however, no AOM activity was detected in $^{14}C\text{-}CH_4$ incubations. It is possible that the ANMEs were present but not active, as the 16S data does not provide direct evidence of metabolic activity. In deeper sediment intervals, two methanogenic families belonging to *Methanosarcinaceae* and *Methanonatronarchaeaceae* were detected. Both these groups are halotolerant and can produce methane from non-competitive substrates and could be responsible for the MG-MMA rates we detected in the deeper sediments at the HP station (Boone et al., 2015; Sorokin et al., 2018).

An alternative hypothesis worth testing in future investigations is that methanogens are potentially responsible at mediating both methanogenesis and AOM of the cryptic methane cycle. Methanogens and ANMEs both carry the Mcr gene that encodes for the methyl coenzyme M, which under the right kinetic conditions can work in both reductive and oxidative directions

(Timmers et al., 2017; Hallam et al., 2003). In addition, methanogenic groups within the *Methanosarcinales* class have been implicated in performing AOM coupled to iron reduction of poorly reactive iron oxides in lake sediment (Bar-Or et al., 2017) and in marine sediment (Yan et al., 2018; Liang et al., 2019). Such an investigation could be particularly interesting for sediment intervals in which we detected simultaneous AOM rates (Fig. 2E, K, and Q), high porewater iron (II) concentrations (Fig. C, I, and O) and ASVs belonging to *Methanosarcinales* (Fig. 5A, B and C). At the HP station, AOM rates were detected in deeper sediment intervals where no ANME ASVs were detected. Here, AOM may also be mediated by groups of methanogens. At 16.5-17.5 cm, *Methanosarcinaceae*, a group within *Methanosarcinales*, was detected and could potentially be involved in AOM similar to the other stations. However, iron (II) concentrations at the HP station were low and it is unclear if iron (III) could be the electron acceptor for AOM at these depths. These data combined, at a minimum, points to the involvement of methanogens with iron-dependent AOM, however, this study did not directly test this hypothesis and future investigations should focus on the how methanogens could be cycling methane with iron as the electron acceptor.

4.4. Indications for rapid turnover of metabolic substrates

Salt marshes are known to be rich in fresh organic matter which consists of competitive and non-competitive substrates for methanogenesis (Yuan et al., 2014; 2019; Wang and Lee, 1994; Fitzsimons et al., 1997; Fitzsimons et al., 2005). Porewater analysis by NMR revealed that porewaters from the BL, BH, and M stations had quantifiable concentrations of acetate. Acetate is a product from fermentation of organic matter by homoacetogenesis (Jørgensen, 2000; Ragsdale and Pierce, 2008). Acetate is an important substrate for a wide range of microbial groups and considered a competitive substrate between methanogenic archaea and sulfate-

reducing bacteria (Jørgensen, 2000; Conrad, 2020). Acetate concentrations that were below quantification or detection (similar to methanol and methylamines) in our study indicate that this substrate could be subject to rapid turnover, similar to what is described for microbial turnover for hydrogen (Conrad, 1999; Hoehler et al., 2001), as it is produced particularly in shallower sediment intervals.

Porewater methanol was mostly below detection and sometimes present but not quantifiable in the CSMR sediment porewater (see section 3.1.4.). Although methanol is known to be a non-competitive substrate for methylotrophic methanogenesis in coastal wetlands (King et al., 1983; Oremland and Polcin, 1982) it has recently been found to be a carbon source for other non-methanogenic metabolisms such as denitrifying and sulfate-reducing bacteria and aerobic and anaerobic methylotrophs (Fischer et al., 2021), which according to our 16S data are likely present in the CSMR (Fig. 6 and 7). Similar to acetate, low or undetectable concentrations of methanol could indicate fast metabolic turnover, as this substrate is expected to be produced in surface sediments of salt marshes (Oremland and Polcin, 1982; Oremland et al., 1982).

Natural porewater MMA concentrations were also mostly below detection (< 3 μM), however, at some depth intervals in the BL and HP stations MMA concentrations were below quantification (<10 μM) (Table 1). It is not possible to report definitive quantities of MMA in this study, however, we can bracket the MMA concentrations in a range between 3 and 10 μM. MMA concentrations in sediment porewaters are still poorly constrained. A previous study of MMA in the Mersey Estuary, UK reports sediment porewater concentrations up to 319 μM (Fitzsimons et al., 1997). Other studies report lower sediment porewater concentrations, for example ~2 μM MMA in the Flax Pond salt Marsh (Wang and Lee, 1994) and between 0.08 and 1.44 μM in the Thames Estuary, UK (Fitzsimons et al., 2006). Non-quantifiable (but detectable)

MMA concentrations in the CSMR sediment porewater may as well indicate rapid consumption by the microbial community and/or binding to mineral surfaces (Wang and Lee, 1990; Xiao et al., 2022). Data from our ^{14}C-MMA incubations provide support for both hypotheses as we observed the metabolic potential for MMA through the turnover of the injected ^{14}C-MMA and found that between 38% and 55% of the injected ^{14}C-MMA bound to the sediment (see Sec. 3.3.1).

At all CSMR stations we found large differences between AOM-CH_4 (i.e., AOM determined based on ^{14}C-TIC production after injection of ^{14}C-CH_4) and AOM-MMA (AOM determined based on ^{14}C-TIC production after injection of ^{14}C-MMA). In intervals where both AOM-CH_4 and AOM-MMA rates were detected, AOM-MMA was 1-2 orders of magnitude higher than AOM-CH_4 (Fig. 2E, K, Q, and W). We suggest the large difference between the two AOM rates is the result of ^{14}C-TIC production from direct oxidation of ^{14}C-MMA by non-methanogenic pathways, similarly to what was previously hypothesized by (Krause et al., 2023). Direct conversion of ^{14}C-MMA to ^{14}C-TIC inflates the rate constants for AOM-MMA dramatically (see Eq. 2). Figure 2F, L, R, and X indeed show that rate constants for AOM-MMA are 1-2 orders of magnitude higher than both MG-MMA and AOM-CH_4. Similar to the interpretations made by Krause et al. (2023), we suggest that the ^{14}C-TIC produced during the ^{14}C-MMA incubations stems only partially from AOM as part of the cryptic methane cycle (i.e., the ^{14}C-CH_4 intermediate). The majority of ^{14}C-MMA was likely subject to direct methylamine oxidation by an unidentified anaerobic methylotrophic metabolism.

Methylamines are the simplest alkylated amine and derived from the degradation of osmolytes found in plant biomass (Oren, 1990; Taubert et al., 2017). Methylamines are ubiquitously found in saline and hypersaline conditions in marine sediments (Zhuang et al.,

2016; Zhuang et al., 2017; Mausz and Chen, 2019) and in coastal wetlands (Fitzsimons et al., 2006; Fitzsimons et al., 2005; Fitzsimons et al., 2001; Fitzsimons et al., 1997). Because methylamine molecules are both a carbon and nitrogen source it is an important food sources for a variety of microbial communities such as aerobic methylotrophic bacteria (Taubert et al., 2017; Chistoserdova, 2015; Hanson and Hanson, 1996) and obligate anaerobic methanogens (Chistoserdova, 2015; Thauer, 1998). However, increasing reports are providing evidence that methylamines may be directly oxidized anaerobically by non-methanogenic metabolisms in anoxic sediment. Krause et al., (2023) provided some literature evidence that implicates sulfate-reducing bacteria and other heterotrophic bacteria maybe responsible for methylamine consumption in hypersaline and marine sediments. Although evidence of non-methanogenic anaerobic methylamine oxidation in wetland sediment is scarce based on the findings in the present study, we suggest that sulfate-reducing bacteria were consuming MMA concurrent with methylotrophic methanogenesis at all studied stations (Fig. 2E, F, K, L, Q, R, W and X). A recent study showed that sulfate-reducing bacteria belonging to the order Desulfobacterales expanded their genetic code to enable the utilization of trimethylamine in a wide range of sediment environments and actively in competition with methylotrophic methanogens (Kivenson et al., 2021). ASVs belonging to the order Desulfobacterales were detected in throughout the sediment intervals across the CSMR transect (Fig. 6A-D), which may be involved with anaerobic methylamine consumption that we observed in our study. However, the present study did not perform transcriptomics to determine if the sulfate-reducers detected in the CSMR transect are expressing metabolic machinery and are actively utilizing methylamines.

Our 16S data also reveal some other potential candidates in methylamine consumption in the CSMR. Fig. 7 shows the relative abundances of bacterial phyla found in the sediment across

the CSMR stations namely, Proteobacteria, Firmicutes, Actinobacteria, Verrucomicrobia, candidate phylum NC10, and Actinobacteriota. These phyla do have representatives that are known to be methylotrophs (Anthony, 1982; Chistoserdova and Lidstrom, 2013; Mctaggart et al., 2015). Interestingly, many of these phyla contain groups of aerobic methylotrophs (Chistoserdova and Lidstrom, 2013) and it is unclear why they would be present in anoxic sulfate and iron-reducing sediment in the CSMR (Fig. 2).

If methylated substrates in anaerobic metabolism are not restricted to methanogenic archaea, then it is crucial to understand how competitive these substrates are between methylotrophic methanogens and other microorganisms. A future hypothesis worth testing is that anaerobic non-methane methylotrophic metabolisms do limit the availability of methylated substrates to methylotrophic methanogenesis in coastal wetland sediment. If proven to be true, it could be an additional contributing reason why coastal wetlands have lower methane emissions to the atmosphere and thus better constrain the global methane budget. The identification of this currently unknown metabolism and the microbial groups responsible, along with the mechanism that drives the competition is especially important because if environmental conditions were to change in favor of methanogenic archaea to convert the methylated substrates to methane, then the question remains whether the cryptic methane cycle that is already present will be amplified or whether there is a greater chance for coastal wetlands to become a methane contributor.

4.5. Implications for cryptic methane cycling in coastal wetlands

Coastal wetlands are at the boundary between terrestrial and marine ecosystems. However, reports showing the decline in coastal wetland areas due to a variety of anthropogenic pressures (i.e., land reclamation, agriculture, and run off) are increasing (Newton et al., 2020). The leading concern is sea-level rise caused by increasing temperatures globally driven by

climate change. The fear is that sea level rise will potentially permanently inundate coastal wetland areas globally. This inundation would then deliver more organic material into coastal wetlands, leading to potentially exhausting electron acceptors thereby changing the redox potential of the sediment and thus promote higher anaerobic metabolic activity and leave more organic matter for methanogenesis in coastal wetland sediment (Liu et al., 2019; Gatland et al., 2014; Zhao et al., 2020; Vizza et al., 2017; Dinsmore et al., 2009). With this imminent problem arising, important questions remain about the effect of climate-induced sea-level rise has on methylotrophic activity and the cryptic methane cycle within coastal wetlands. A future hypothesis worth testing is that inundation of coastal wetlands due to sea-level rise enhances cryptic methane cycling activity (elevated methanogenesis and AOM activity) supported by large pools of electron acceptors found in the subsurface porewaters. If confirmed, with the evidence presented in this study, the cryptic methane cycle maybe enhanced during periods of extended inundation, keeping methane concentrations low and therefore a lower emission of a potent greenhouse gas.

5. Conclusions

In the present study, we set about to find spatial evidence of the cryptic methane cycle and potential microbial communities involved, within the top 20 cm of sediment along a land-ocean transect within the CSMR, using a variety of geochemical and molecular analytics. We found overlap of methylotrophic methanogenesis and AOM activities within the top 15-20 cm at the BL, BH, and M stations and below 8 cm at the HP station. We conclude that the cryptic methane cycle is active keeping methane concentrations present but low across the CSMR transect. We found that the CSMR hydrology dynamics at the surface is different to the subsurface hydrology, particularly at the brackish stations suggesting that more inland portions of the CSMR may have once been more hypersaline. In parallel, porewater sulfate concentrations were not limiting and supported sulfate reduction rates and likely AOM. However, porewater iron (II) concentrations and the detection of ASV's belonging to iron reducers indicate that iron reduction could too be an important metabolism and potentially be coupled to AOM, which needs further investigation to confirm. Metabolomic analysis of porewater indicate a rapid production and consumption of methylated substrates for methanogenesis. Molecular analysis detected methanogenic archaea at all stations along the transect, but methanotrophic archaea only in the M and HP stations, suggesting that cryptic methane cycling could be facilitated by either a methanogen-methanotroph archaea couple or by putative methanogenic archaea that are capable of both processes. Our rate data strongly suggest that not only is cryptic methane cycling active in the CSMR sediment, but there is also an unknown anaerobic methylotrophic metabolism directly oxidizing methylamine into the inorganic carbon pool. Our molecular analysis along with literature evidence implicate sulfate-reducing bacteria within the order Desulfobacterales could be responsible for the turnover of methylated substrates, but more work is needed to

confirm. Our study emphasizes the biogeochemical complexity occurring in the sediment across spatial gradients within a coastal wetland. Future work should investigate further the mechanisms that lead to the production and consumption of methylated substrates like methylamine and how that may affect the cryptic methane cycle. Such investigations may provide additional reasons why coastal wetlands do not emit as much methane to the atmosphere and questions the long-standing notion of the exclusivity of methylated substrates for methanogenesis.

Acknowledgements

The authors thank the University of California Natural Reserve System and the Project Scientist of the Carpinteria Salt Marsh Reserve, A. Brooks, for authorizing the field sampling in June 2019. We acknowledge X. Hwang for providing fieldwork and laboratory instrument support. We acknowledge S. Connon and S. Lim for providing laboratory and sequencing analysis support. This work received financial support through the University of California and the National Science Foundation (NSF) (Award No.: 1852912).

References

Anthony, C.: The biochemistry of methylotrophs, 1982.

Aromokeye, D. A., Kulkarni, A. C., Elvert, M., Wegener, G., Henkel, S., Coffinet, S., Eickhorst, T., Oni, O. E., Richter-Heitmann, T., and Schnakenberg, A.: Rates and microbial players of iron-driven anaerobic oxidation of methane in methanic marine sediments, Frontiers in Microbiology, 10, 487993, 2020.

Bar-Or, I., Elvert, M., Eckert, W., Kushmaro, A., Vigderovich, H., Zhu, Q., Ben-Dov, E., and Sivan, O.: Iron-coupled anaerobic oxidation of methane performed by a mixed bacterial-archaeal community based on poorly reactive minerals, Environmental science & technology, 51, 12293-12301, 2017.

Barnes, R. O. and Goldberg, E. D.: Methane production and consumption in anoxic marine sediments, Geology, 4, 297-300, 1976.

Bartlett, K. B., Bartlett, D. S., Harriss, R. C., and Sebacher, D. J.: Methane emissions along a salt marsh salinity gradient, Biogeochemistry, 4, 183-202, 1987.

Bartoli, M., Nizzoli, D., Zilius, M., Bresciani, M., Pusceddu, A., Bianchelli, S., Sundbäck, K., Razinkovas-Baziukas, A., and Viaroli, P.: Denitrification, nitrogen uptake, and organic matter quality undergo different seasonality in sandy and muddy sediments of a turbid estuary, Frontiers in microbiology, 11, 612700, 2021.

Beal, E. J., House, C. H., and Orphan, V. J.: Manganese- and iron-dependent marine methane oxidation, Science, 325, 184-187, 2009.

Bernard, B. B.: Methane in marine sediments, Deep Sea Research Part A. Oceanographic Research Papers, 26, 429-443, 1979.

Beulig, F., Røy, H., McGlynn, S. E., and Jørgensen, B. B.: Cryptic CH4 cycling in the sulfate-methane transition of marine sediments apparently mediated by ANME-1 archaea, The ISME journal, https://doi.org/10.1038/s41396-41018-40273-z, 2018.

Boetius, A., Ravenschlag, K., Schubert, C. J., Rickert, D., Widdel, F., Giesecke, A., Amann, R., Jørgensen, B. B., Witte, U., and Pfannkuche, O.: A marine microbial consortium apparently mediating anaerobic oxidation of methane, Nature, 407, 623-626, 2000.

Booij, K., Helder, W., and Sundby, B.: Rapid redistribution of oxygen in a sandy sediment induced by changes in the flow velocity of the overlying water, Netherlands Journal of Sea Research, 28, 149-165, 1991.

Boone, D. R., Whitman, W. B., and Koga, Y.: Methanosarcinaceae, Bergey's Manual of Systematics of Archaea and Bacteria, 1-2, 2015.

Boudreau, B. P., Huettel, M., Forster, S., Jahnke, R. A., McLachlan, A., Middelburg, J. J., Nielsen, P., Sansone, F., Taghon, G., and Van Raaphorst, W.: Permeable marine sediments: overturning an old paradigm, EOS, Transactions American Geophysical Union, 82, 133-136, 2001.

Bridgham, S., Cadillo-Quiroz, H., Keller, J., and Zhuang, Q.: Methane emissions from wetlands: biogeochemical, microbial, and modeling perspectives from local to global scales, Global Change Biology, 19, 1325-1346, 10.1111/gcb.12131, 2013.

Bridgham, S., Megonigal, J., Keller, J., Bliss, N., and Trettin, C.: The carbon balance of North American wetlands, Wetlands, 26, 889-916, 10.1672/0277-5212(2006)26[889:TCBONA]2.0.CO;2, 2006.

Callahan, B. J., McMurdie, P., Rosen, M., Han, A., and Johnson, A.: JA, Holmes SP. 2016, DADA2: high-resolution sample inference from Illumina amplicon data. Nature Methods, 13, 581-583, 2016.
Cao, M., Xin, P., Jin, G., and Li, L.: A field study on groundwater dynamics in a salt marsh–Chongming Dongtan wetland, Ecological Engineering, 40, 61-69, 2012.
Carol, E. S., Kruse, E. E., and Pousa, J. L.: Influence of the geologic and geomorphologic characteristics and of crab burrows on the interrelation between surface water and groundwater in an estuarine coastal wetland, Journal of Hydrology, 403, 234-241, 2011.
Carol, E. S., Dragani, W. C., Kruse, E. E., and Pousa, J. L.: Surface water and groundwater characteristics in the wetlands of the Ajó River (Argentina), Continental Shelf Research, 49, 25-33, 2012.
Chen, S., Torres, R., and Goñi, M. A.: The role of salt marsh structure in the distribution of surface sedimentary organic matter, Estuaries and coasts, 39, 108-122, 2016.
Chistoserdova, L.: Methylotrophs in natural habitats: current insights through metagenomics, Applied microbiology and biotechnology, 99, 5763-5779, 2015.
Chistoserdova, L. and Lidstrom, M. E.: Aerobic methylotrophic prokaryotes, The prokaryotes, 267-285, 2013.
Cline, J. D.: Spectrophometric determination of hydrogen sulfide in natural waters, Limnol. Oceanogr., 14, 454-458, 1969.
Conrad, R.: Contribution of hydrogen to methane production and control of hydrogen concentrations in methanogenic soils and sediments, FEMS microbiology Ecology, 28, 193-202, 1999.
Conrad, R.: Importance of hydrogenotrophic, aceticlastic and methylotrophic methanogenesis for methane production in terrestrial, aquatic and other anoxic environments: a mini review, Pedosphere, 30, 25-39, 2020.
Dale, A. W., Sommer, S., Lomnitz, U., Montes, I., Treude, T., Liebetrau, V., Gier, J., Hensen, C., Dengler, M., Stolpovsky, K., Bryant, L. D., and Wallmann, K.: Organic carbon production, mineralisation and preservation on the Peruvian margin, Biogeosciences, 12, 1537-1559, 2015.
de los Santos, C. B., Egea, L. G., Martins, M., Santos, R., Masqué, P., Peralta, G., Brun, F. G., and Jiménez-Ramos, R.: Sedimentary organic carbon and nitrogen sequestration across a vertical gradient on a temperate wetland seascape including salt marshes, seagrass meadows and rhizophytic macroalgae beds, Ecosystems, 26, 826-842, 2023.
del Pilar Alvarez, M., Carol, E., Hernández, M. A., and Bouza, P. J.: Groundwater dynamic, temperature and salinity response to the tide in Patagonian marshes: Observations on a coastal wetland in San José Gulf, Argentina, Journal of South American Earth Sciences, 62, 1-11, 2015.
Diao, M., Dyksma, S., Koeksoy, E., Ngugi, D. K., Anantharaman, K., Loy, A., and Pester, M.: Global diversity and inferred ecophysiology of microorganisms with the potential for dissimilatory sulfate/sulfite reduction, FEMS Microbiology Reviews, 47, fuad058, 2023.
Dinsmore, K. J., Skiba, U. M., Billett, M. F., and Rees, R. M.: Effect of water table on greenhouse gas emissions from peatland mesocosms, Plant and Soil, 318, 229-242, 2009.
Egger, M., Hagens, M., Sapart, C. J., Dijkstra, N., van Helmond, N. A., Mogollón, J. M., Risgaard-Petersen, N., van der Veen, C., Kasten, S., and Riedinger, N.: Iron oxide reduction in

methane-rich deep Baltic Sea sediments, Geochimica et Cosmochimica Acta, 207, 256-276, 2017.
Egger, M., Rasigraf, O., Sapart, C. J., Jilbert, T., Jetten, M. S., Rockmann, T., Van der Veen, C., Banda, N., Kartal, B., and Ettwig, K. F.: Iron-mediated anaerobic oxidation of methane in brackish coastal sediments, Environmental Science & Technology, 49, 277-283, 2015.
Ettwig, K. F., Zhu, B., Speth, D., Keltjens, J. T., Jetten, M. S., and Kartal, B.: Archaea catalyze iron-dependent anaerobic oxidation of methane, Proceedings of the National Academy of Sciences, 113, 12792-12796, 2016.
Fischer, P. Q., Sánchez‐Andrea, I., Stams, A. J., Villanueva, L., and Sousa, D. Z.: Anaerobic microbial methanol conversion in marine sediments, Environmental microbiology, 23, 1348-1362, 2021.
Fitzsimons, M., Dawit, M., Revitt, D., and Rocha, C.: Effects of early tidal inundation on the cycling of methylamines in inter-tidal sediments, Marine Ecology Progress Series, 294, 51-61, 2005.
Fitzsimons, M. F., Jemmett, A. W., and Wolff, G. A.: A preliminary study of the geochemistry of methylamines in a salt marsh, Organic geochemistry, 27, 15-24, 1997.
Fitzsimons, M. F., Kahni-danon, B., and Dawitt, M.: Distributions and adsorption of the methylamines in the inter-tidal sediments of an East Anglian Estuary, Environm. Experiment. Bot., 46, 225-236, 2001.
Fitzsimons, M. F., Millward, G. E., Revitt, D. M., and Dawit, M. D.: Desorption kinetics of ammonium and methylamines from estuarine sediments: consequences for the cycling of nitrogen, Marine Chemistry, 101, 12-26, 2006.
Gardner, L. R.: Role of stratigraphy in governing pore water seepage from salt marsh sediments, Water Resources Research, 43, 2007.
Gatland, J. R., Santos, I. R., Maher, D. T., Duncan, T., and Erler, D. V.: Carbon dioxide and methane emissions from an artificially drained coastal wetland during a flood: Implications for wetland global warming potential, Journal of Geophysical Research: Biogeosciences, 119, 1698-1716, 2014.
Goslin, J., Sansjofre, P., Van Vliet‐Lanoë, B., and Delacourt, C.: Carbon stable isotope (δ 13C) and elemental (TOC, TN) geochemistry in saltmarsh surface sediments (Western Brittany, France): a useful tool for reconstructing Holocene relative sea‐level, Journal of Quaternary Science, 32, 989-1007, 2017.
Grasshoff, K., Ehrhardt, M., and Kremling, K.: Methods of seawater analysis, Wiley-VCH Verlag GmbH, Weinheim1999.
Hallam, S. J., Girguis, P. R., Preston, C. M., Richardson, P. M., and DeLong, E. F.: Identification of methyl coenzym m reductase A (mcrA) genes associated with methane-oxidizing archaea, Appl. Environ. Microbiol., 69, 5483-5491, 2003.
Hanson, R. S. and Hanson, T. E.: Methanotrophic bacteria, Microbiol. Rev., 60, 439-471, 1996.
Hinrichs, K.-U. and Boetius, A.: The anaerobic oxidation of methane: new insights in microbial ecology and biogeochemistry, in: Ocean Margin Systems, edited by: Wefer, G., Billett, D., Hebbeln, D., Jørgensen, B. B., Schlüter, M., and Van Weering, T., Springer-Verlag, Berlin, 457-477, 2002.

Hoehler, T. M., Alperin, M. J., Albert, D. B., and Martens, C. S.: Apparent minimum free energy requirements for methanogenic Archaea and sulfate-reducing bacteria in an anoxic marine sediment, FEMS Microbiol. Ecol., 38, 33-41, 2001.
Holmes, D. E., Nicoll, J. S., Bond, D. R., and Lovley, D. R.: Potential role of a novel psychrotolerant member of the family Geobacteraceae, Geopsychrobacter electrodiphilus gen. nov., sp. nov., in electricity production by a marine sediment fuel cell, Applied and Environmental Microbiology, 70, 6023-6030, 2004.
Huettel, M., Ziebis, W., and Forster, S.: Flow - induced uptake of particulate matter in permeable sediments, Limnology and Oceanography, 41, 309-322, 1996.
Huettel, M., Ziebis, W., Forster, S., and Luther, I. G. W.: Advective transport affecting metal and nutrient distribution and interfacial fluxes in permeable sediments, Geochim. Cosmochim. Acta, 62, 613-631, 1998.
IPCC, C. C.: Mitigation of climate change, Contribution of working group III to the fifth assessment report of the intergovernmental panel on climate change, 2014.
Iversen, N. and Jørgensen, B. B.: Diffusion coefficients of sulfate and methane in marine sediments: influence of porosity, Geochim. Cosmochim. Acta, 57, 571-578, 1993.
Jackson, K. L., Whitcraft, C. R., and Dillon, J. G.: Diversity of Desulfobacteriaceae and overall activity of sulfate-reducing microorganisms in and around a salt pan in a southern California coastal wetland, Wetlands, 34, 969-977, 2014.
Joye, S. B., Boetius, A., Orcutt, B. N., Montoya, J. P., Schulz, H. N., Erickson, M. J., and Logo, S. K.: The anaerobic oxidation of methane and sulfate reduction in sediments from Gulf of Mexico cold seeps, Chem. Geol., 205, 219-238, 2004.
Jørgensen, B. B.: A comparison of methods for the quantification of bacterial sulphate reduction in coastal marine sediments: I. Measurements with radiotracer techniques, Geomicrobiol. J., 1, 11-27, 1978.
Jørgensen, B. B.: Bacteria and marine biogeochemistry, in: Marine biogeochemistry, edited by: Schulz, H. D., and Zabel, M., Springer Verlag, Berlin, 173-201, 2000.
Kallmeyer, J., Ferdelman, T. G., Weber, A., Fossing, H., and Jørgensen, B. B.: A cold chromium distillation procedure for radiolabeled sulfide applied to sulfate reduction measurements, Limnol. Oceanogr. Methods, 2, 171-180, 2004.
King, G., Klug, M. J., and Lovley, D. R.: Metabolism of acetate, methanol, and methylated amines in intertidal sediments of Lowes Cove, Maine, 45, 1848-1853, 1983.
Kivenson, V., Paul, B. G., and Valentine, D. L.: An ecological basis for dual genetic code expansion in marine deltaproteobacteria, Frontiers in microbiology, 1545, 2021.
Knittel, K. and Boetius, A.: Anaerobic oxidation of methane: progress with an unknown process, Annu. Rev. Microbiol., 63, 311-334, 2009.
Knudsen, M.: Hydrographical Tables According to the Measurings of Carl Forch...[et Al.] and with Assistance of Björn-Andersen...[et Al.], GEC Gad1901.
Kostka, J. E., Roychoudhury, A., and Van Cappellen, P.: Rates and controls of anaerobic microbial respiration across spatial and temporal gradients in saltmarsh sediments, Biogeochemistry, 60, 49-76, 2002.
Krause, S. J. and Treude, T.: Deciphering cryptic methane cycling: Coupling of methylotrophic methanogenesis and anaerobic oxidation of methane in hypersaline coastal wetland sediment, Geochimica et Cosmochimica Acta, 302, 160-174, 2021.

Krause, S. J., Liu, J., Yousavich, D. J., Robinson, D., Hoyt, D. W., Qin, Q., Wenzhöfer, F., Janssen, F., Valentine, D. L., and Treude, T.: Evidence of cryptic methane cycling and non-methanogenic methylamine consumption in the sulfate-reducing zone of sediment in the Santa Barbara Basin, California, Biogeosciences, 20, 4377-4390, 2023.
Kristjansson, J. K., Schönheit, P., and Thauer, R. K.: Different Ks values for hydrogen of methanogenic bacteria and sulfate reducing bacteria: an explanation for the apparent inhibition of methanogenesis by sulfate, Arch. Microbiol., 131, 278-282, 1982.
La, W., Han, X., Liu, C.-Q., Ding, H., Liu, M., Sun, F., Li, S., and Lang, Y.: Sulfate concentrations affect sulfate reduction pathways and methane consumption in coastal wetlands, Water Research, 217, 118441, 2022.
Li, Y., Wang, D., Chen, Z., Chen, J., Hu, H., and Wang, R.: Methane emissions during the tide cycle of a Yangtze Estuary salt marsh, Atmosphere, 12, 245, 2021.
Li, Z., Hodges, B. R., and Shen, X.: Modeling hypersalinity caused by evaporation and surface–subsurface exchange in a coastal marsh, Journal of Hydrology, 618, 129268, 2023.
Liang, L., Wang, Y., Sivan, O., and Wang, F.: Metal-dependent anaerobic methane oxidation in marine sediment: Insights from marine settings and other systems, Science China Life Sciences, 62, 1287-1295, 2019.
Liu, L., Wang, D., Chen, S., Yu, Z., Xu, Y., Li, Y., Ge, Z., and Chen, Z.: Methane emissions from estuarine coastal wetlands: Implications for global change effect, Soil Science Society of America Journal, 83, 1368-1377, 2019.
Liu, Y. and Whitman, W. B.: Metabolic, phylogenetic, and ecological diversity of the methanogenic archaea, Annals of the new York Academy of Sciences, 1125, 171-189, 2008.
Lovley, D.: Dissimilatory Fe (III)-and Mn (IV)-reducing prokaryotes, Prokaryotes, 2, 635-658, 2006.
Lovley, D. R. and Klug, M. J.: Model for the distribution of sulfate reduction and methanogenesis in freshwater sediments, Geochim. Cosmochim. Acta, 50, 11-18, 1986.
Lovley, D. R. and Phillips, E. J.: Competitive mechanisms for inhibition of sulfate reduction and methane production in the zone of ferric iron reduction in sediments, Applied and Environmental Microbiology, 53, 2636-2641, 1987.
Maltby, J., Sommer, S., Dale, A., and Treude, T.: Microbial methanogenesis in the sulfate-reducing zone of surface sediments traversing the Peruvian margin, Biogeosciences, 13, 283-299, 10.5194/bg-13-283-2016, 2016.
Martin, M.: Cutadapt removes adapter sequences from high-throughput sequencing reads, EMBnet. journal, 17, 10-12, 2011.
Martinez-Cruz, K., Sepulveda-Jauregui, A., Casper, P., Anthony, K. W., Smemo, K. A., and Thalasso, F.: Ubiquitous and significant anaerobic oxidation of methane in freshwater lake sediments, Water research, 144, 332-340, 2018.
Mausz, M. A. and Chen, Y.: Microbiology and ecology of methylated amine metabolism in marine ecosystems, Current Issues in Molecular Biology, 33, 133-148, 2019.
McTaggart, T. L., Beck, D. A., Setboonsarng, U., Shapiro, N., Woyke, T., Lidstrom, M. E., Kalyuzhnaya, M. G., and Chistoserdova, L.: Genomics of methylotrophy in Gram-positive methylamine-utilizing bacteria, Microorganisms, 3, 94-112, 2015.
Meyers, P. A.: Preservation of elemental and isotopic source identification of sedimentary organic matter, Chemical geology, 114, 289-302, 1994.

Michaelis, W., Seifert, R., Nauhaus, K., Treude, T., Thiel, V., Blumenberg, M., Knittel, K., Gieseke, A., Peterknecht, K., Pape, T., Boetius, A., Aman, A., Jørgensen, B. B., Widdel, F., Peckmann, J., Pimenov, N. V., and Gulin, M.: Microbial reefs in the Black Sea fueled by anaerobic oxidation of methane, Science, 297, 1013-1015, 2002.
Moffett, K. B., Robinson, D. A., and Gorelick, S. M.: Relationship of salt marsh vegetation zonation to spatial patterns in soil moisture, salinity, and topography, Ecosystems, 13, 1287-1302, 2010.
Montalto, F. A., Steenhuis, T. S., and Parlange, J.-Y.: The hydrology of Piermont Marsh, a reference for tidal marsh restoration in the Hudson river estuary, New York, Journal of Hydrology, 316, 108-128, 2006.
Motelica-Heino, M., Naylor, C., Zhang, H., and Davison, W.: Simultaneous release of metals and sulfide in lacustrine sediment, Environmental Science & Technology, 37, 4374-4381, 2003.
Newton, A., Icely, J., Cristina, S., Perillo, G. M., Turner, R. E., Ashan, D., Cragg, S., Luo, Y., Tu, C., and Li, Y.: Anthropogenic, direct pressures on coastal wetlands, Frontiers in Ecology and Evolution, 8, 144, 2020.
Oksanen, J., Blanchet, F. G., Kindt, R., Legendre, P., Minchin, P. R., O'hara, R., Simpson, G. L., Solymos, P., Stevens, M. H. H., and Wagner, H.: Package 'vegan', Community ecology package, version, 2, 1-295, 2013.
Oremland, R. S. and Polcin, S.: Methanogenesis and sulfate reduction: competitive and noncompetitive substrates in estuarine sediments, Appl. Environ. Microbiol., 44, 1270-1276, 1982.
Oremland, R. S. and Taylor, B. F.: Sulfate reduction and methanogenesis in marine sediments, Geochimica et Cosmochimica Acta, 42, 209-214, 1978.
Oremland, R. S., Marsh, L. M., and Polcin, S.: Methane production and simultaneous sulphate reduction in anoxic, salt marsh sediments, Nature, 296, 143-145, 1982.
Oren, A.: Formation and breakdown of glycine betaine and trimethylamine in hypersaline environments, Antonie van Leeuwenhoek, 58, 291-298, 1990.
Oren, A.: The family methanoregulaceae, The prokaryotes: other major lineages of bacteria and the archaea, 253-258, 2014.
Orphan, V. J., House, C. H., Hinrichs, K.-U., McKeegan, K. D., and De Long, E. F.: Methane-consuming Archaea revealed by directly coupled isotopic and phylogenetic analysis, Science, 293, 484-487, 2001.
Park, H. S., Lin, S., and Voordouw, G.: Ferric iron reduction by Desulfovibrio vulgaris Hildenborough wild type and energy metabolism mutants, Antonie Van Leeuwenhoek, 93, 79-85, 2008.
Parkes, R. J., Brock, F., Banning, N., Hornibrook, E. R., Roussel, E. G., Weightman, A. J., and Fry, J. C.: Changes in methanogenic substrate utilization and communities with depth in a salt-marsh, creek sediment in southern England, Estuarine, Coastal and Shelf Science, 96, 170-178, 2012.
Postma, D. and Jakobsen, R.: Redox zonation: equilibrium constraints on the Fe (III)/SO4-reduction interface, Geochimica et Cosmochimica Acta, 60, 3169-3175, 1996.
Precht, E., Franke, U., Polerecky, L., and Huettel, M.: Oxygen dynamics in permeable sediments with wave-driven pore water exchange, Limnol. Oceanogr., 49, 693-705, 2004.

Quast, C., Pruesse, E., Yilmaz, P., Gerken, J., Schweer, T., Yarza, P., Peplies, J., and Glöckner, F. O.: The SILVA ribosomal RNA gene database project: improved data processing and web-based tools, Nucleic acids research, 41, D590-D596, 2012.
Ragsdale, S. W. and Pierce, E.: Acetogenesis and the Wood–Ljungdahl pathway of CO2 fixation, Biochimica et Biophysica Acta (BBA)-Proteins and Proteomics, 1784, 1873-1898, 2008.
Reddy, K. R. and DeLaune, R. D.: Biogeochemistry of Wetlands, CRC Press, Taylor & Francis Group, Boca Raton, 756 pp.2008.
Reddy, K. R., DeLaune, R. D., and Inglett, P. W.: Biogeochemistry of wetlands: science and applications, CRC press2022.
Reeburgh, W. S.: Oceanic methane biogeochemistry, Chem. Rev., 107, 486-513, 2007.
Reyes, C., Schneider, D., Thürmer, A., Kulkarni, A., Lipka, M., Sztejrenszus, S. Y., Böttcher, M. E., Daniel, R., and Friedrich, M. W.: Potentially active iron, sulfur, and sulfate reducing bacteria in Skagerrak and Bothnian Bay sediments, Geomicrobiology Journal, 34, 840-850, 2017.
Rocha, C.: Rhythmic ammonium regeneration and flushing in intertidal sediments of the Sado estuary, Limnology and Oceanography, 43, 823-831, 1998.
Rooze, J., Egger, M., Tsandev, I., and Slomp, C. P.: Iron‐dependent anaerobic oxidation of methane in coastal surface sediments: Potential controls and impact, Limnology and Oceanography, 61, S267-S282, 2016.
Rusch, A., Forster, S., and Huettel, M.: Bacteria, diatoms and detritus in an intertidal sandflat subject to advective transort across the water-sediment interface, Biogeochemistry, 55, 1-27, 2001.
Saunois, M., Stavert, A. R., Poulter, B., Bousquet, P., Canadell, J. G., Jackson, R. B., Raymond, P. A., Dlugokencky, E. J., Houweling, S., and Patra, P. K.: The global methane budget 2000–2017, Earth system science data, 12, 1561-1623, 2020.
Scheller, S., Yu, H., Ghadwick, G. L., McGlynn, S. E., and Orphan, V. J.: Artificial electron acceptors decouple archaeal methane oxidation from sulfate reduction, Science, 351, 703-707, 2016.
Segarra, K. E., Comerford, C., Slaughter, J., and Joye, S. B.: Impact of electron acceptor availability on the anaerobic oxidation of methane in coastal freshwater and brackish wetland sediments, Geochimica et Cosmochimica Acta, 115, 15-30, 2013.
Sorokin, D. Y., Merkel, A. Y., Abbas, B., Makarova, K. S., Rijpstra, W. I. C., Koenen, M., Sinninghe Damsté, J. S., Galinski, E. A., Koonin, E. V., and Van Loosdrecht, M. C.: Methanonatronarchaeum thermophilum gen. nov., sp. nov. and'Candidatus Methanohalarchaeum thermophilum', extremely halo (natrono) philic methyl-reducing methanogens from hypersaline lakes comprising a new euryarchaeal class Methanonatronarchaeia classis nov, International journal of systematic and evolutionary microbiology, 68, 2199-2208, 2018.
Taubert, M., Grob, C., Howat, A. M., Burns, O. J., Pratscher, J., Jehmlich, N., von Bergen, M., Richnow, H. H., Chen, Y., and Murrell, J. C.: Methylamine as a nitrogen source for microorganisms from a coastal marine environment, Environmental microbiology, 19, 2246-2257, 2017.

Thauer, R. K.: Biochemistry of methanogenesis: a tribute to Marjory Stephenson, Microbiology, 144, 2377-2406, 1998.
Tilbrook, B. D. and Karl, D. M.: Methane sources, distributions and sinks from California coastal waters to the oligotrophic North Pacific gyre, Marine Chemistry, 49, 51-64, 1995.
Timmers, P. H. A., Welte, C. U., Koehorst, J. J., Plugge, C. M., Jetten, M. S. M., and Stams, A. J. M.: Reverse methanogenesis and respiration in methanotrophic archaea, Archaea, Article ID 1654237, 2017.
Treude, T., Krüger, M., Boetius, A., and Jørgensen, B. B.: Environmental control on anaerobic oxidation of methane in the gassy sediments of Eckernförde Bay (German Baltic), Limnol. Oceanogr., 50, 1771-1786, 2005.
Valenzuela, E. I., Avendaño, K. A., Balagurusamy, N., Arriaga, S., Nieto-Delgado, C., Thalasso, F., and Cervantes, F. J.: Electron shuttling mediated by humic substances fuels anaerobic methane oxidation and carbon burial in wetland sediments, Science of The Total Environment, 650, 2674-2684, 2019.
Vizza, C., West, W. E., Jones, S. E., Hart, J. A., and Lamberti, G. A.: Regulators of coastal wetland methane production and responses to simulated global change, Biogeosciences. 14 (2): 431-446., 14, 431-446, 2017.
Waite, D. W., Chuvochina, M., Pelikan, C., Parks, D. H., Yilmaz, P., Wagner, M., Loy, A., Naganuma, T., Nakai, R., and Whitman, W. B.: Proposal to reclassify the proteobacterial classes Deltaproteobacteria and Oligoflexia, and the phylum Thermodesulfobacteria into four phyla reflecting major functional capabilities, International Journal of Systematic and Evolutionary Microbiology, 70, 5972-6016, 2020.
Wallenius, A. J., Dalcin Martins, P., Slomp, C. P., and Jetten, M. S.: Anthropogenic and environmental constraints on the microbial methane cycle in coastal sediments, Frontiers in Microbiology, 12, 631621, 2021.
Wang, X.-c. and Lee, C.: The distribution and adsorption behavior of aliphatic amines in marine and lacustrine sediments, Geochimica et Cosmochimica Acta, 54, 2759-2774, 1990.
Wang, X.-C. and Lee, C.: Adsorption and desorption of aliphatic amines, amino acids and acetate by clay minerals and marine sediments, Marine Chemistry, 44, 1-23, 1993.
Wang, X.-C. and Lee, C.: Sources and distribution of aliphatic amines in salt marsh sediment, Organic Geochemistry, 22, 1005-1021, 1994.
Weber, K. A., Achenbach, L. A., and Coates, J. D.: Microorganisms pumping iron: anaerobic microbial iron oxidation and reduction, Nature Reviews Microbiology, 4, 752-764, 2006.
Wehrmann, L. M., Risgaard-Petersen, N., Schrum, H. N., Walsh, E. A., Huh, Y., Ikehara, M., Pierre, C., D'Hondt, S., Ferdelman, T. G., and Ravelo, A. C.: Coupled organic and inorganic carbon cycling in the deep subseafloor sediment of the northeastern Bering Sea Slope (IODP Exp. 323), Chemical Geology, 284, 251-261, 2011.
Winfrey, M. R. and Ward, D. M.: Substrates for sulfate reduction and methane p roduction in i ntertidal sediments, Appl. Environm. Microbiol, 45, 193-199, 1983.
Xia, S., Song, Z., Li, Q., Guo, L., Yu, C., Singh, B. P., Fu, X., Chen, C., Wang, Y., and Wang, H.: Distribution, sources, and decomposition of soil organic matter along a salinity gradient in estuarine wetlands characterized by C: N ratio, δ13C - δ15N, and lignin biomarker, Global Change Biology, 27, 417-434, 2021.

Xiao, K., Beulig, F., Roy, H., Jorgensen, B., and Risgaard-Petersen, N.: Methylotrophic methanogenesis fuels cryptic methane cycling in marine surface sediment, Limnology and Oceanography, 63, 1519-1527, 10.1002/lno.10788, 2018.
Xiao, K.-Q., Beulig, F., Kjeldsen, K. U., Jørgensen, B. B., and Risgaard-Petersen, N.: Concurrent methane production and oxidation in surface sediment from Aarhus Bay, Denmark, Frontiers Microbiol., 8, doi: 10.3389/fmicb.2017.01198, 2017.
Xiao, K.-Q., Moore, O. W., Babakhani, P., Curti, L., and Peacock, C. L.: Mineralogical control on methylotrophic methanogenesis and implications for cryptic methane cycling in marine surface sediment, Nature Communications, 13, 1-9, 2022.
Yan, Z., Joshi, P., Gorski, C. A., and Ferry, J. G.: A biochemical framework for anaerobic oxidation of methane driven by Fe (III)-dependent respiration, Nature communications, 9, 1642, 2018.
Young, C. M.: Reproduction, development and life-history traits, in: Deep-sea ecosystems, edited by: Tyler, P. A., Ecosystems of the world, Elsevier, Amsterdam, 2003.
Yuan, J., Ding, W., Liu, D., Xiang, J., and Lin, Y.: Methane production potential and methanogenic archaea community dynamics along the Spartina alterniflora invasion chronosequence in a coastal salt marsh, Applied microbiology and biotechnology, 98, 1817-1829, 2014.
Yuan, J., Liu, D., Ji, Y., Xiang, J., Lin, Y., Wu, M., and Ding, W.: Spartina alterniflora invasion drastically increases methane production potential by shifting methanogenesis from hydrogenotrophic to methylotrophic pathway in a coastal marsh, Journal of Ecology, 107, 2436-2450, 2019.
Zhao, M., Han, G., Li, J., Song, W., Qu, W., Eller, F., Wang, J., and Jiang, C.: Responses of soil CO2 and CH4 emissions to changing water table level in a coastal wetland, Journal of Cleaner Production, 269, 122316, 2020.
Zhuang, G.-C., Elling, F. J., Nigro, L. M., Samarkin, V., Joye, S. B., Teske, A., and Hinrichs, K.-U.: Multiple evidence for methylotrophic methanogenesis as the dominant methanogenic pathway in hypersaline sediments from the Orca Basin, Gulf of Mexico, Geochim. Cosmochim. Acta, 187, 1-20, 2016.
Zhuang, G.-C., Lin, Y.-S., Bowles, M. W., Heuer, V. B., Lever, M. A., Elvert, M., and Hinrichs, K.-U.: Distribution and isotopic composition of trimethylamine, dimethylsulfide and dimethylsulfoniopropionate in marine sediments, Mar. Chem., 196, 35-46, 2017.
Zhuang, G.-C., Heuer, V. B., Lazar, C. S., Goldhammer, T., Wendt, J., Samarkin, V. A., Elvert, M., Teske, A. P., Joye, S. B., and Hinrichs, K.-U.: Relative importance of methylotrophic methanogenesis in sediments of the Western Mediterranean Sea, Geochim. Cosmochim. Acta, 224, 2018.
Ziebis, W., Huettel, M., and Forster, S.: The impact of biogenic sediment topography on oxygen fluxes in permeable sediments, Mar. Ecol. Prog. Ser., 140, 227-237, 1996.

Supplemental Material

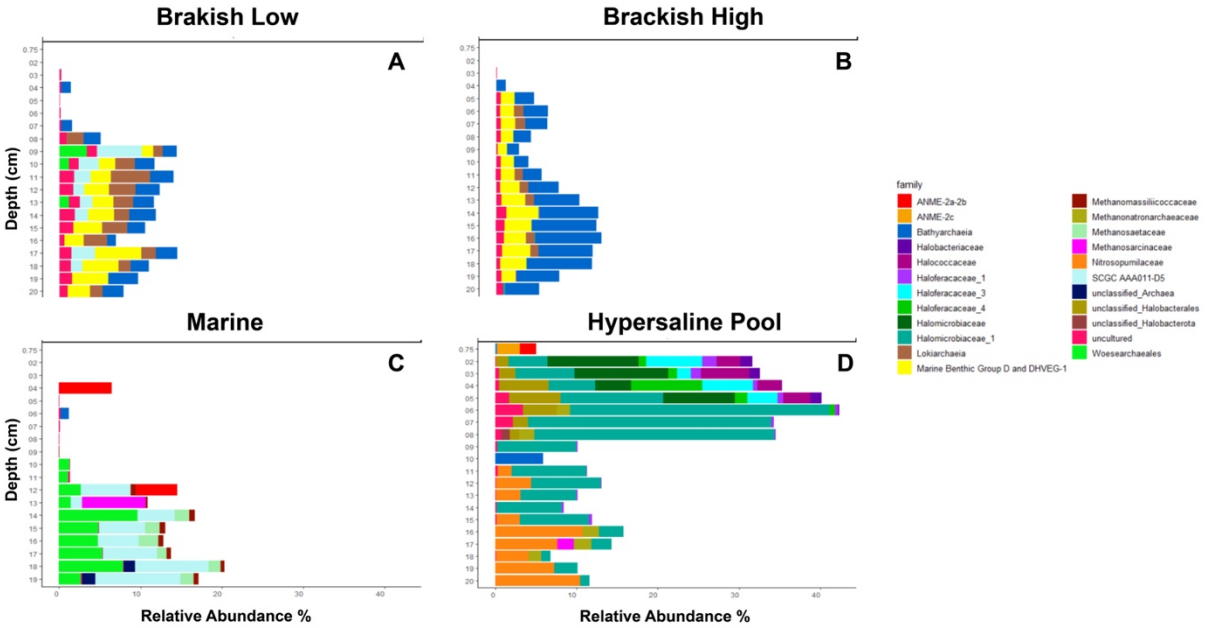

Figure S1. Relative abundances of the top 23 archaeal families detected in the sediment along the CSMR transect.